



# On the generality of a preferred orientation at interfaces of crystals

Catherine Zhou, Gregory S. Rohrer, Paul A. Salvador<sup>ID</sup>\*

Department of Materials Science and Engineering, Carnegie Mellon University, 5000 Forbes Ave., Pittsburgh, 15213, PA, USA

## ARTICLE INFO

### Keywords:

Solid interfaces  
Epitaxy of thin films  
Grain boundaries

## ABSTRACT

The generality of a preferred orientation at crystalline interfaces is considered by analyzing previously reported computed grain boundary energies of metals from an epitaxial thin film perspective. 388 *fcc* and 408 *bcc* boundaries are sorted in a fashion that is conceptually analogous to combinatorial substrate epitaxy (*CSE*) experiments previously reported for non-isostructural oxide film–substrate pairs. *CSE* observations are briefly reviewed, indicating that there is a single preferred *OR* for all film–substrate pairs of close-packed oxides, regardless of the interface plane, which is called the eutactic *OR*. The eutactic *OR* is shown to be structurally similar to the  $\Sigma 3$  coincident site lattice (*CSL*) *OR* for grain boundaries of metals. Based on low-energy outliers in the grain boundary populations, it is shown that the  $\Sigma 3$  *CSL* *OR* (the common twin misorientation) is the preferred *OR* for both metal families, also regardless of the interface orientation. The combined observations for metal grain boundaries and epitaxial oxide films are consistent with the existence of a single preferred *OR* (a  $\Sigma 3$  *OR*) at interfaces of crystals.

## 1. Introduction

Crystalline interfaces are of great scientific interest because they are known to control both important material processes, such as nucleation and growth [1–3], and material properties, from mechanical behavior [4,5] to superconductivity [6–8]. Two of the most well-studied crystalline interfaces are epitaxial interfaces [3,9–12], or the planar boundary between materials involved in the well-ordered crystalline growth of a film on a substrate, and grain boundaries [5,13–16], or the planar boundary between volumes of a material having different crystallographic orientations (grains). In general, these different interface types are treated separately by their respective scientific communities. There are clear distinctions between the crystallographic selection events that occur during the formation of these two interface types, resulting in seemingly disconnected outcomes. During epitaxial growth, high-energy adatoms attach to a substrate that has a fixed orientation and surface plane and select an orientation that provides the lowest energy (within the constraints of kinetics) [3,17,18]. During grain boundary formation, crystals with fixed 3D orientations impinge upon one another and select the habit plane that provides the lowest energy (within the constraints of the entire grain boundary network and kinetics) [14,19–21]. Both communities focus on similar questions: What are the preferred low-energy interfaces and why? Despite years of study, many outstanding fundamental questions persist, including: is there a general preferred orientation relationship between crystals at interfaces? We will provide evidence that the answer to this is yes,

specifically  $\Sigma 3$  *ORs*, and discuss the crystallographic nature of the preferred *ORs*.

This has traditionally been a challenging question to address because of the large number of distinct interfaces in materials. One must define at least five independent parameters, which can be represented as angles, to describe the structure of a crystalline interface [5,13,14,22]. Three parameters are related to the misorientation of the two crystals (or the orientation relationship, which is denoted herein as the *OR*) and two are related to the orientation of the interface plane [14,22]. Even considering reasonable resolution values for each parameter and taking into account symmetry-based reductions, a very large number (thousands to millions) of distinct interfaces can be delineated for grain or phase boundaries [22]. Thus, historical investigations of interfaces usually restricted the type of interface investigated and narrowed the range of parameter space explored, focusing on more specific questions than the general ones posed above.

Over the past few decades, significant progress has been made in high-throughput characterization methods that allow for the extraction of populations and energies over the five-dimensional parameter space of interfaces. These methods were developed primarily to characterize grain boundaries [14,22], but were later extended to investigate epitaxial films [24–26]. High-throughput observations of epitaxial thin film growth (called combinatorial substrate epitaxy or *CSE*) of structurally dissimilar film–substrate pairs indicate that there is a single, simple, preferred 3D *OR* across orientation space and film–substrate pairs. This

\* Corresponding author.

E-mail address: [paulsalvador@cmu.edu](mailto:paulsalvador@cmu.edu) (P.A. Salvador).

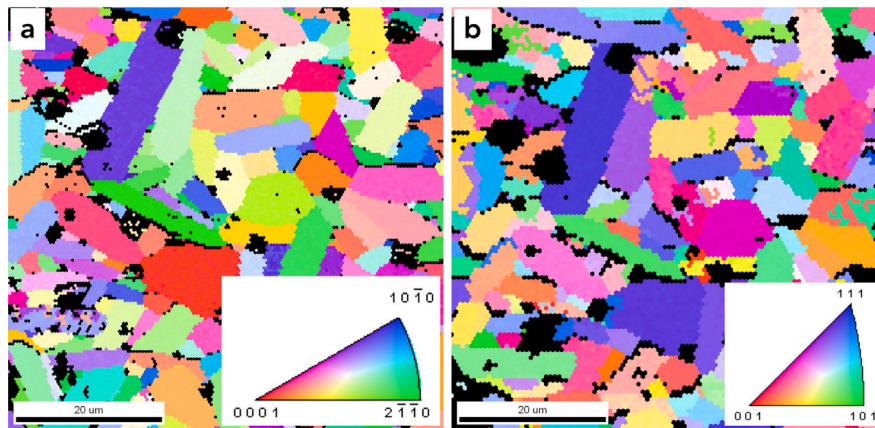


**Fig. 1.** Orientation (inverse pole figure) maps of (a) a 4H SrMnO<sub>3</sub> substrate and (b) a 3C CaMnO<sub>3</sub> film deposited on the same region of the substrate. Orientation color keys given as insets.

Source: Reproduced with permission from [23].

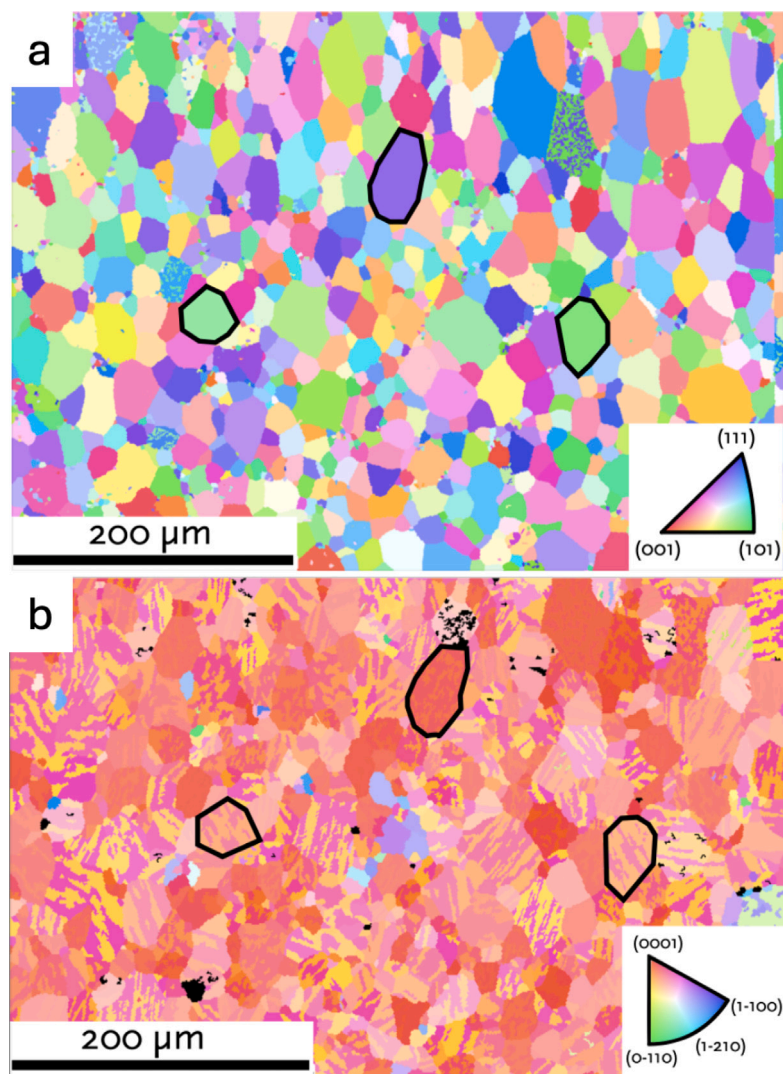


**Fig. 2.** Orientation (inverse pole figure) maps of (a) a 3C SrTiO<sub>3</sub> substrate and (b) a 2H hematite Fe<sub>2</sub>O<sub>3</sub> film deposited on the same region of the substrate. Orientation color keys given as insets.

Source: Reproduced with permission from [24].

preferred OR is called the eutactic OR [24], where the eutactic (nearly close-packed [27]) planes and directions are aligned in 3D. This is reviewed in Section 2 where this OR is shown to be structurally similar to a  $\Sigma 3$  coincident site lattice (CSL) OR in metals. While CSE observations provide empirical evidence that there is a preferred OR at crystalline interfaces during film growth, such evidence has not been observed for grain boundaries. High-throughput computations have also allowed for the determination of a large number of grain boundary energies (and mobilities), and these generally reinforce experimental observations, but they have not indicated that a preferred OR (or misorientation) exists at grain boundaries.

In this work, evidence supporting a preferred OR at grain boundaries is presented, regardless of the nature of the interface plane. Several publicly available computed grain boundary energy datasets for *fcc* [28,29] and *bcc* metals [30] are recast as hypothetical thin film (CSE) experiments. Results from those hypothetical CSE experiments strongly support that the so-called  $\Sigma 3$  OR (or the common twin misorientation) is the preferred OR at grain boundaries in both *fcc* and *bcc* materials, regardless of the selection of a given interface plane itself. In addressing the preferred OR, which can be described as a  $\Sigma 3$  CSL for both epitaxial interfaces (of eutactic oxides) and grain boundaries (of *fcc* and *bcc* metals), it will be shown that being structurally similar in 3D appears to be essential in generating the lowest energy interface for an arbitrary selection of an interface plane.

## 2. The preferred eutactic OR in oxide epitaxy

### 2.1. CSE and 3D ORs

Combinatorial substrate epitaxy (CSE) [23–26,31–37] is a high-throughput thin film deposition method in which the substrate is a dense polycrystalline compact that is cut, thinned, and polished to be epitaxy ready (i.e., processed in a manner similar to single crystals typically used for epitaxial growth). Each grain at the substrate surface can be considered as an individual single crystal with an orientation that is essentially independent of the other grains, and thousands of crystals are present in a typical CSE substrate. When considering the ensemble of individual crystals available for growth, one can survey the entire orientation space within a single CSE deposition. Structural characterization is carried out using electron backscatter diffraction (EBSD).

As examples, inverse pole figure maps from 4H perovskite SrMnO<sub>3</sub> and 3C perovskite SrTiO<sub>3</sub> polycrystalline substrates are shown in Fig. 1(a) [23] and Fig. 2(a) [24], respectively. Inverse pole figure map from a 3C perovskite CaMnO<sub>3</sub> film deposited on the 4H-SrMnO<sub>3</sub> substrate, and a hematite (2H) Fe<sub>2</sub>O<sub>3</sub> film on the 3C perovskite SrTiO<sub>3</sub> substrate, are shown respectively in Fig. 1(b) [23] and Fig. 2(b) [24] (note that the 2H, 3C, and 4H notation will be described in Section 2.2). It is clear that: (1) grain shapes are largely retained between the image pairs, indicating grain-over-grain growth, and (2) grains usually have one color, indicating local epitaxial growth.

Because most substrate crystals have general surfaces with low 2D symmetry, epitaxial ORs in CSE focus on overall 3D ORs, similar to that done in the grain boundary community, rather than the in-plane 2D relationships focused on in traditional single-crystal epitaxy [3,9–12,17,18,38]. Fig. 3 shows the angle between the stacking directions of (i.e., normals to) the eutactic (nearly close-packed [27]) planes/directions of: (a) the 3C CaMnO<sub>3</sub> film ([111]/[110]) on the 4H SrMnO<sub>3</sub> substrate ([001]/[100]) in black/red, and (b) the 2H Fe<sub>2</sub>O<sub>3</sub> film ([001]/[100]) on the 3C SrTiO<sub>3</sub> substrate ([111]/[110]) in blue/red. The average angle (standard deviation) between the eutactic planar normals/directions is (ignoring outliers): (a) 2.6° (0.4°) / 1.8° (0.7°) and (b) 4.2° (6.5°) / 3.0° (5.2°).

This epitaxial OR, called the eutactic OR [24], was observed for (a) 98% of 90 [23] and (b) 92% of 500 [24] film–substrate grain pairs, regardless of interface plane, indicating it represents a higher-level 3D

driving force for epitaxy. Importantly, the interface plane does not appear to have a large impact on the average epitaxial OR, indicating that this OR is the preferred OR at all eutactic interfaces, including semi-coherent or incoherent ones.

### 2.2. The generality of the eutactic OR and its connection to the $\Sigma 3$ CSL OR

The eutactic OR has been consistently observed as the preferred OR in CSE experiments. CSE experiments have been carried out for various non-isostructural eutactic oxide films on polycrystalline substrates, including: anatase/rutile TiO<sub>2</sub> on perovskite BaTiO<sub>3</sub> [25] and BiFeO<sub>3</sub> [26], hematite Fe<sub>2</sub>O<sub>3</sub> on perovskite SrTiO<sub>3</sub> [24], scrutinyite/rutile SnO<sub>2</sub> on columbite CoNb<sub>2</sub>O<sub>6</sub> [36], and 3C and 4H perovskite AEMnO<sub>3</sub> (AE = Ca, Sr) on 3C SrTiO<sub>3</sub> and 4H SrMnO<sub>3</sub> [23,37], as well as other isostructural films–substrates combinations [31–35]. Across most of the CSE investigations on non-isostructural film–substrate pairs, there is only one preferred 3D-OR for each film–substrate structural pair, the eutactic OR, regardless of the 2D surface structure on which the film grew.

Schematic overlays of the 3D crystal structures are given in Fig. 4 for (a) 3C–4H structures (such as CaMnO<sub>3</sub>–SrMnO<sub>3</sub>) and (b) 3C–2H structures (such as SrTiO<sub>3</sub>–Fe<sub>2</sub>O<sub>3</sub>). In both, the vertical direction corresponds to the stacking direction of the eutactic planes, which are (111) for 3C and (001) for 4H and 2H. The atom locations within a eutactic plane are given as the letters adjacent to the planes, and the viewing direction is parallel to the eutactic direction within the plane, such that atom locations coincident in the viewing plane are also coincident everywhere along the viewing direction. The eutactic planes have a stoichiometry of AO<sub>3</sub> for perovskites or O<sub>4</sub> for other eutactic oxides (including corundum, rutile, anatase, etc.). For the eutactic ORs shown, 1/3 of all lattice sites are coincident in 3D, which can be observed when the eutactic planes have identical atom positions within the stacking plane (i.e., the same stacking letter). Thus, all eutactic planes can be described as coincident (*c*) or non-coincident (*n*). For the (a) 3C–4H pair, there is a 12 plane repeat of *cnmnnccnmmnn* (or a 1-4-3-4 alternation of planes of *c-n-c-n*). For the (b) 3C–2H pair, there is a 6 plane repeat of *cnmnn* (or a 2–4 alternation of planes of *c-n*).

This leads to the hypothesis that the eutactic  $\Sigma 3$  is the lowest-energy OR regardless of the substrate or film material (at least for eutactic polymorphs), or their specific bulk or interfacial structures. In other words, the eutactic OR has the lowest energy interface, regardless of the absolute value of the energy, which may be high on semi-coherent or incoherent interfaces. Schematic interfaces between a 4H substrate (blue spheres) and a 3C film (red spheres) are given in Fig. 5, for three eutactic OR interfaces. In (a), the eutactic planes are parallel to each other at the interface, yielding an interface with 100% coincident sites; one expects this to be low energy. In (b) and (c), the eutactic planes are denoted as the slanted lines that cross the interfaces. They both have an interfacial coincidence for 1/3 of the eutactic planes, in patterns expected from those of the 3D  $\Sigma 3$  patterns described above. Whether (b) and (c) should be the lowest-energy interfaces for those substrate planes is impossible to discern from the images.

An extension of the eutactic OR hypothesis is that there is a general preferred 3D-OR at all crystal interfaces, including grain boundaries, and that the preferred OR is the  $\Sigma 3$  OR (and the eutactic OR is a type of  $\Sigma 3$  OR). Unfortunately, there are no experimental or computational datasets for the energy of epitaxial interfaces across orientation space. A direct test of the extended hypothesis would be to compare the energies of a large number of different grain boundaries (for which there are large datasets) when sorted in the fashion of a CSE experiment, which is the focus of rest of this paper.

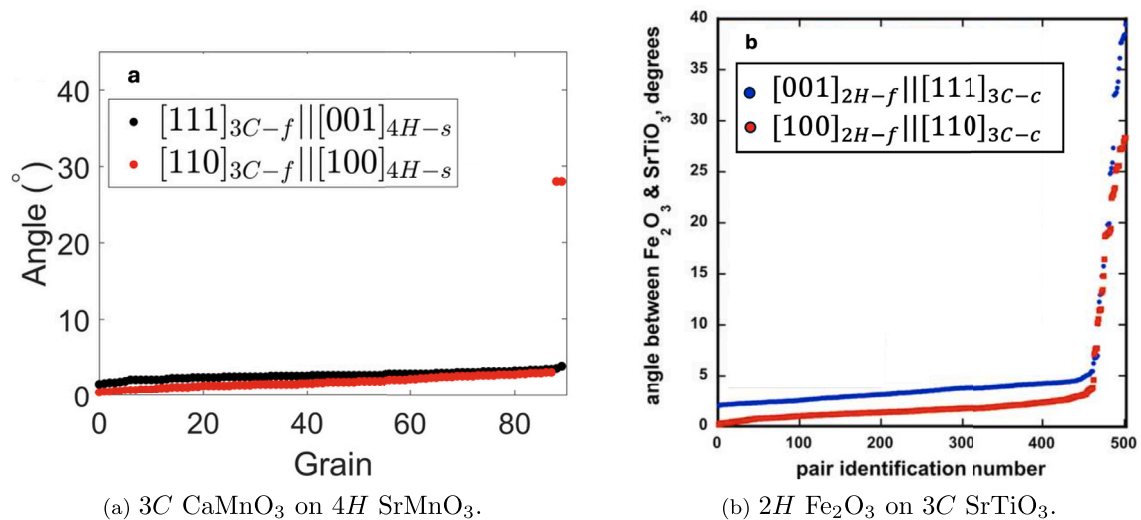


**Fig. 3.** Angle between eutactic planes and directions for: (a) a 3C CaMnO<sub>3</sub> film on a 4H SrMnO<sub>3</sub> polycrystalline substrate (from Fig. 1) and (b) a 2H Fe<sub>2</sub>O<sub>3</sub> film on a 3C SrTiO<sub>3</sub> substrate (from Fig. 2). Black dots in (a) (blue in (b)) represent the angles between the normals of eutactic planes of the film and the substrate and red dots in both represent the angles between the eutactic directions in those planes. Insets give indices of specific planes and directions. *f* stands for film and *s* stands for substrate (on left). (For interpretation of the references to color in this figure legend, the reader is referred to the web version of this article.)  
Source: Reproduced with permission from [23] (left) and [24] (right).

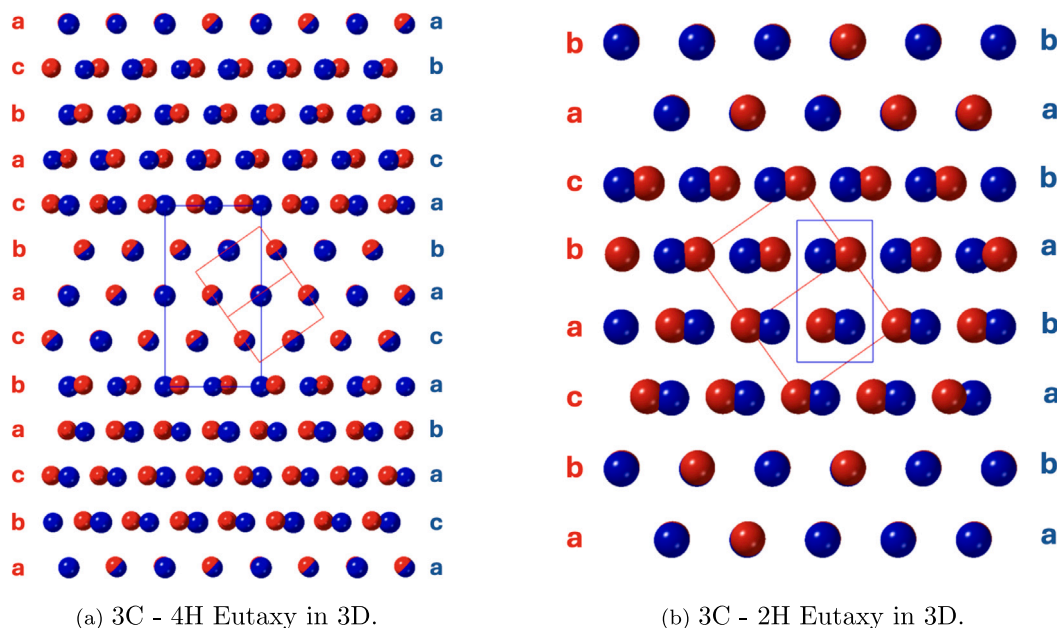


**Fig. 4.** 3D schematics of two different eutactic structural pairs, focusing on the stacking of the close-packed planes (either O<sub>4</sub> or AO<sub>3</sub>) in the vertical direction. For the 3C (4H and 2H) grains, the [111], [110], and [112] ([001], [010], and [210]) are vertical, into the page, and horizontal. The 3C stacking is shown in red as *abc* with red spheres and the (a) 4H or (b) 2H stacking is shown in blue as (a) *acab* and (b) *ab* with blue spheres. Overall, both end up as  $\Sigma 3$  CSLs, but with different sequences of coincident (c) and non-coincident (n) eutactic planes: (a) *cnnnccnncnnn* and (b) *cnnnn*. (For interpretation of the references to color in this figure legend, the reader is referred to the web version of this article.)

### 3. The preferred OR at grain boundaries

#### 3.1. $\Sigma 3$ OR for *fcc* and *bcc* grain boundaries

Schematic overlays of the 3D crystal structures for two grains with a  $\Sigma 3$  OR are shown in Fig. 6 for (a) *fcc* grains (Ni and Al) and (b) *bcc* grains (Fe and Mo). In both, the vertical direction corresponds to the stacking of the (111) planes (the  $\Sigma 3$  OR can be considered a rotation of the second grain by 60° about the [111], resulting in an inversion domain along [111]). The atom locations within a (111) plane are given as the letters adjacent to the planes in (a) (numbers in (b)), and the viewing direction is parallel to the [110] direction within the plane, such that atom locations coincident in the viewing plane

are also coincident everywhere along the viewing direction. 1/3 of all lattice sites are coincident in 3D, which can be observed when the (111) planes have identical atom positions within the stacking plane (i.e., the same stacking letter/number). Thus, (111) planes can be described as coincident (c) or non-coincident (n). For both  $\Sigma 3$  ORs, there is a 3 plane repeat of *cnn* (or a 1–2 alternation of planes of c-n). The grain boundary crystallography shown in Fig. 6 for  $\Sigma 3$  ORs is similar to that shown in Fig. 4 for eutactic ORs, where the grain boundaries have the smallest possible repeat period between coincident planes of 3 planes in the stacking direction. Although the *fcc* structure is eutactic, the *bcc* structure is not. This will help differentiate between a eutactic OR preference or a  $\Sigma 3$  OR preference.

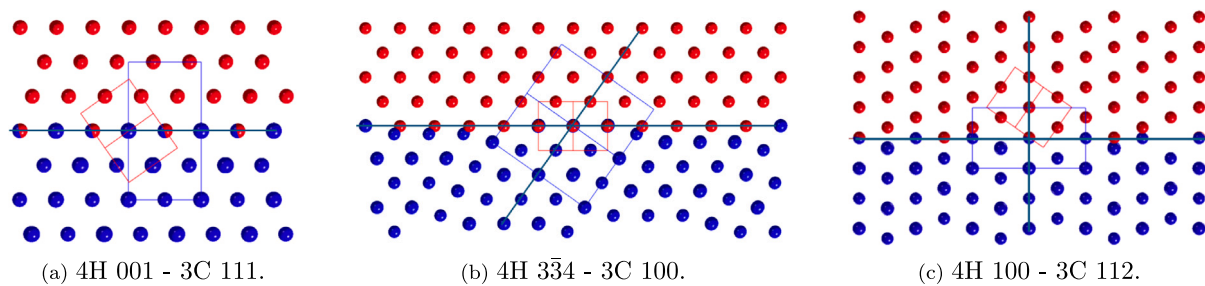


**Fig. 5.** Schematic interfaces between a 4H substrate (blue spheres) and a 3C film plane (red spheres). The interface plane is marked as the horizontal line and the eutactic plane is marked as the same in (a) and the slanted lines in (b) and (c). The interface arrangements are shown in sub-captions. Unit cells are shown in each, with an  $\langle 010 \rangle$  and a  $\langle 1\bar{1}0 \rangle$  pointing into the page respectively for the 4H and 3C. All atoms in (a) are coincident at the interface, while  $1/3$  of the atoms are coincident in (b,c), in similar patterns to the (111) stacking sequence discussed in Fig. 4. (For interpretation of the references to color in this figure legend, the reader is referred to the web version of this article.)

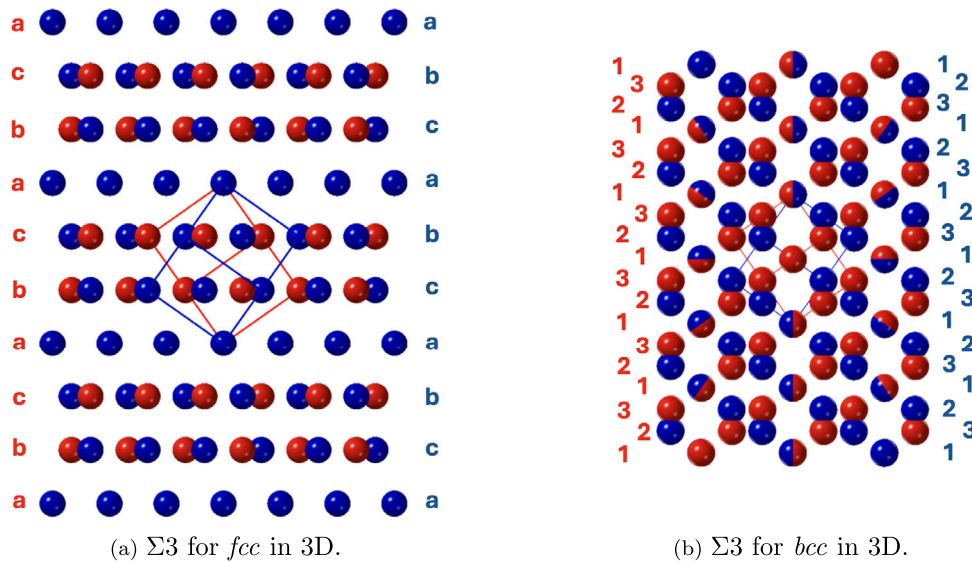


**Fig. 6.** 3D schematics of the  $\Sigma 3$  ORs for (a) *fcc* and (b) *bcc* metals, focusing on the stacking of the (111) planes: the [111], [110], and [112] are vertical, into the page, and horizontal. The (111) planar stacking sequences are shown in red (*abc* or *123*) for the grain with red spheres and in blue (*acb* or *132*) for the grain with blue spheres. Overall, both  $\Sigma 3$  CSLs have identical sequences of coincident (c) and non-coincident (n) (111) planes: *cnm*. (For interpretation of the references to color in this figure legend, the reader is referred to the web version of this article.)

To reinforce the similarity between the eutactic OR at epitaxial interfaces and the  $\Sigma 3$  OR at grain boundaries, schematic interfaces between an *fcc* substrate grain (blue spheres) and an *fcc* film grain (red spheres) are given in Fig. 7, for three  $\Sigma 3$  OR interfaces. In (a), the (111) planes (which are eutactic planes) are parallel to each other at the interface, producing an interface with 100% coincident sites; one expects this to be low energy. In (b) and (c), the (111) planes are denoted as the slanted lines that intersect the interfaces. In (b), which is a twin boundary, there is also complete coincidence of the atoms on (111) planes at the interface plane, but only one of the last three atoms on any (111) plane is at a lattice site. In (c),  $1/3$  of the (111) planes are coincident at the interface, in patterns expected from those of the 3D  $\Sigma 3$  patterns described above. Whether (b) and (c) should be the lowest-energy interfaces for those substrate planes is also impossible to discern from the images.

### 3.2. Computed grain boundary energies

Because of the similarities between the eutactic OR in epitaxy and the  $\Sigma 3$  OR of grain boundaries, it is of interest to recast grain boundary energies as epitaxial films. Two previous publications reported the computed energies for 388 boundaries in *fcc* crystals (Al and Ni) and 408 grain boundaries in *bcc* crystals (Fe and Mo), and those data sets were made available for further exploration [28,30]. Grain pairs (left

and right along the *x*-direction) were constructed having grain boundary planes  $\{hkl\}$  whose normals are in the *x*-direction. Their ORs (or misorientations) were reported as  $\Sigma N$  CSL values. The *N* value in a  $\Sigma N$  CSL boundary corresponds to the inverse number of lattice sites ( $1/N$ ) coincident between the two 3D lattices of the different grains [39,40]. A low *N* value (*N* must be odd) corresponds to more coincident sites in 3D. The lowest possible *N* value is 3, which represents the highest possible number of coincident sites (ignoring  $\Sigma 1$  which represents the perfect crystal).

The grain boundary energies computed in [30] for *bcc* iron are plotted versus  $\Sigma$  value in Fig. 8 (the same is given for *fcc* Ni [28] in Figure S1). Note the wide spread in the  $\Sigma 3$  values for both systems and that some of the lowest energy *bcc*  $\Sigma 3$  boundaries have different planes of high Miller indices. In *bcc*, there is a general low energy of  $\{110\}\{110\}$  grain boundaries, though the lowest  $\{110\}\{110\}$  boundary is also  $\Sigma 3$  (in *fcc* there is a general low energy of  $\{111\}$  twist grain boundaries, whose lowest energy value is the  $\Sigma 3$  coherent twin). Some of the relevant conclusions for *bcc* crystals were: energies ‘are influenced more by the grain boundary plane orientation than by the lattice misorientation or lattice coincidence,’ and boundaries with (110) ‘planes on both sides of the boundary have low energies, regardless of the misorientation angle or geometric character’ [30]. Some of the relevant conclusions for *fcc* crystals were: ‘none of the usual geometric properties associated with grain boundary energy are useful predictors,’ [of energy] and ‘grain boundary energy does not correlate

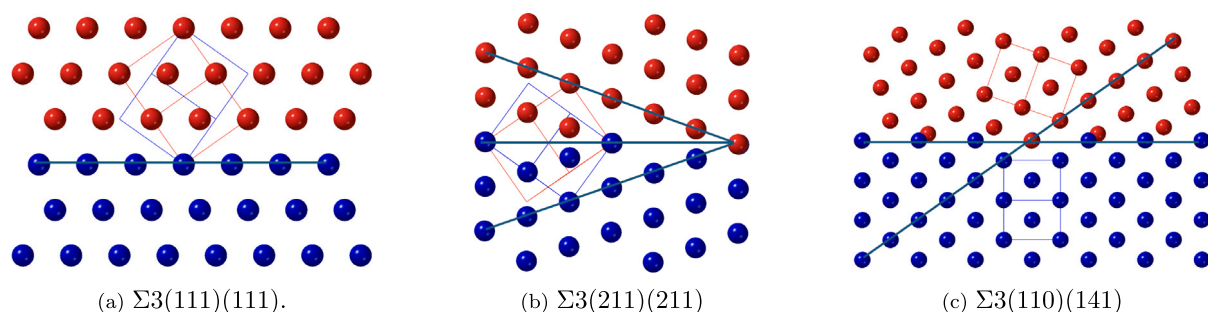


Fig. 7. Schematic interfaces for a  $\Sigma 3$  OR with different interfaces. The blue spheres represent the substrate orientation (first plane listed) and the red spheres represent the film orientation (second plane listed). The interface plane is marked as the horizontal line and the (111) plane is marked as the same in (a) and the slanted lines in (b) and (c). The interface arrangements are shown in sub-captions. Unit cells are shown in each, with a  $\langle 110 \rangle$  pointing into the page. All atoms in (a) are coincident at the interface, while  $1/3$  of the atoms are coincident in (b,c), in similar patterns to the (111) stacking sequence discussed in Fig. 4. (For interpretation of the references to color in this figure legend, the reader is referred to the web version of this article.)

with  $\Sigma$  value, and there is a wide variation in energy for the same  $\Sigma$  value' [28]. Importantly, the datasets were not interrogated with respect to answering whether there was a preferred misorientation for any or all habit planes, as observed for epitaxial interfaces in CSE. This is the subject of the next section.

### 3.3. Hypothetical CSE with grain boundaries

Using the grain boundary energy datasets described above, a hypothetical combinatorial substrate epitaxy (CSE) experiment was constructed. One of the grains (left or right) was considered the substrate, and the other (right or left) was considered the film. The substrate-film interface in this hypothetical CSE experiment was therefore simply the computed grain boundary, and the substrate surface orientation was the habit plane of the substrate grain. For every grain boundary in the published data sets, two substrate-film pairs were considered for inclusion in the CSE data sets. All unique substrate grains were retained in the CSE data set (i.e., the unique orientations of grain boundary normals for both left and right grains). For all unique substrate orientations, the unique film orientations for that substrate orientation were retained in the data set as substrate-film pairs. The total number of *fcc* (*bcc*) substrate-film orientation pairs is 480 (522). The unique substrate grains were further binned into groups according to the number of  $\Sigma 3$  boundaries: those substrates having two or more films with  $\Sigma 3$  ORs, those having one film with a  $\Sigma 3$  OR, and those having no films with a  $\Sigma 3$  OR. Once binned in this CSE fashion, the energies were compared as a function of orientation.

The design of this experiment approximates non-isostructural epitaxy in CSE. It is assumed that the lowest-energy grain boundary for a given substrate plane represents the orientation that one would observe as a hypothetical epitaxial film, among the orientations represented in the dataset. However, not all substrate orientations have all  $\Sigma N$  values computed, so there are some missing low-energy possibilities. Nevertheless, a clear trend in the data for a preferred OR is expected to correlate with CSE observations. If there is a preferred OR, then one OR will be the lowest energy OR, regardless of the substrate plane. The  $\Sigma 3$  OR was shown to be analogous to the preferred eutactic OR in oxide CSE, with  $\Sigma 3$  hypothesized as being preferred because it has the most coincident lattice sites in 3D (Figs. 4 and 6), resulting in interfaces with high lattice site coincidence (Figs. 5 and 7).

### 3.4. Energies in grain boundary CSE

The grain boundary energies are plotted as a function of the angle between the substrate surface plane normal and the normal to the (100) in Figs. 9 and 10, for Ni and Fe, respectively. For simplicity, only plots for Ni (*fcc*) and Fe (*bcc*) are shown; those for Al (*fcc*) and Mo (*bcc*)

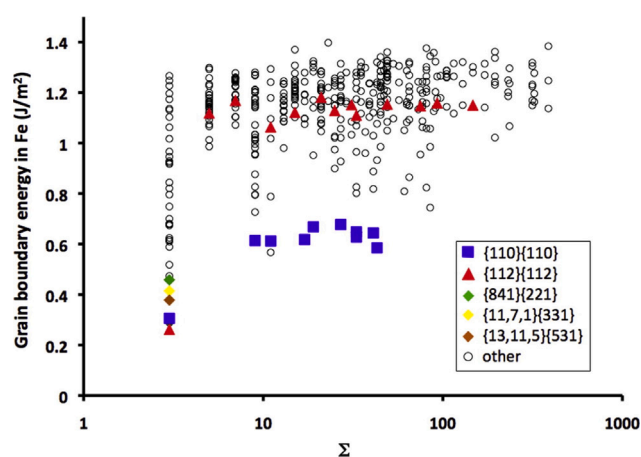
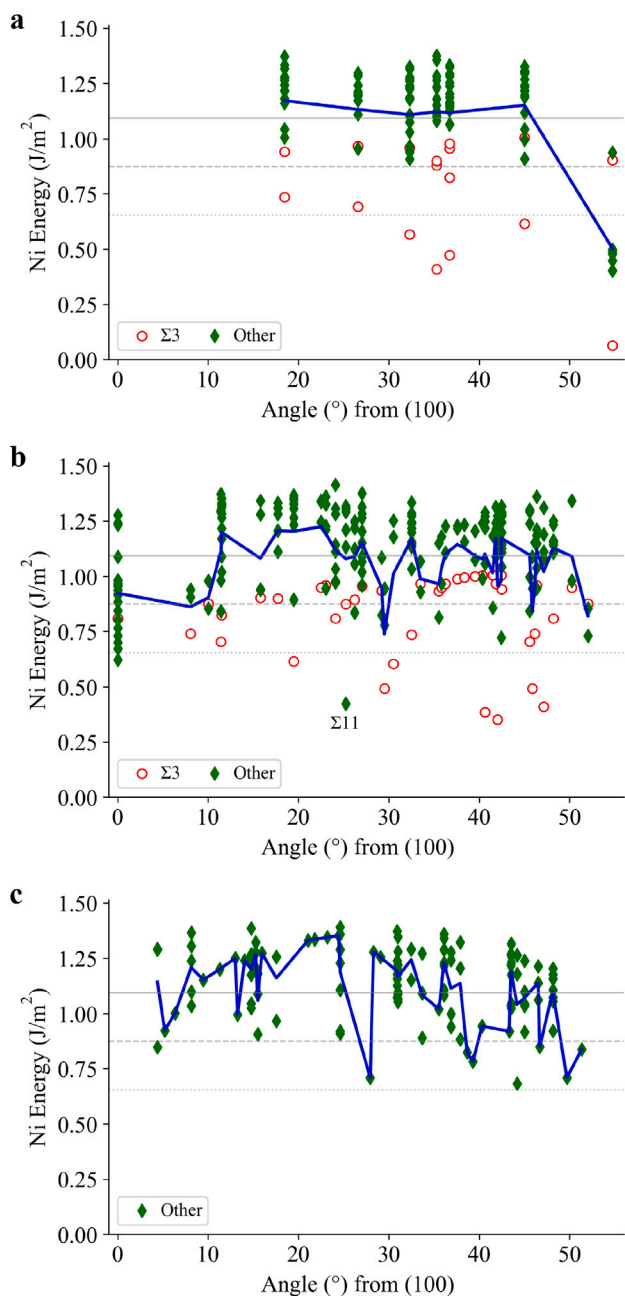


Fig. 8. Grain boundary energy plotted as a function of  $\Sigma$  values ( $N$ ) for *bcc* Fe. The legend indicates the planes of select boundaries.

Source: Reproduced with permission from [30].

are given in Figure S2 and S3 respectively, and values are distributed similarly, but on different energetic scales. In all panels,  $\Sigma 3$  boundaries are plotted as red circles and all other boundaries are plotted as green diamonds. In both figures, panel a, b, and c respectively include only orientations with two or more, one, or no computed  $\Sigma 3$  boundaries. The average value for each orientation in each plot are connected using blue lines. Furthermore, in each panel, the global grain boundary average is plotted as solid gray lines, while the dashed and dotted gray lines indicate values that are respectively one and two standard deviations away from the global average. For *fcc* structures, the global Ni (Al) grain boundary average was  $1.09 \pm 0.22$  J/m<sup>2</sup> ( $0.42 \pm 0.08$  J/m<sup>2</sup>). For *bcc* structures, the global Fe (Mo) grain boundary average was  $1.11 \pm 0.21$  J/m<sup>2</sup> ( $1.59 \pm 0.30$  J/m<sup>2</sup>). Note that because substrate grain orientations have both original left and right grain orientations, when they are unique, the calculation for the global average sometimes contains multiples of the same energy if the film grains were differently oriented. There is a preponderance of  $\Sigma 3$  boundaries below the average, and the preponderance increases as one moves to one then two standard deviations below the average.

The minimum grain boundary energies for a given orientation are plotted as a function of the angle between the substrate surface plane normal and the normal to the (100) in Figs. 11(a) and 11(b), respectively for Ni and Fe. Similar plots are given in Figures S4 and S5 for Al and Mo, respectively. Red circles (blue squares) indicate  $\Sigma 3$  (other types of  $\Sigma N$ ) grain boundaries. The gray solid line indicates the average energy of all minimum energies over all orientations. The dashed



**Fig. 9.** Substrate (left grain boundary) orientations relative to the angle from (100) vs. grain boundary energy ( $\text{J}/\text{m}^2$ ) for *fcc* Ni. (a), (b), and (c), are respectively for orientations with two or more, one, and no  $\Sigma 3$  boundaries calculated. Red circles (green diamonds) indicate  $\Sigma 3$  boundaries (all other boundaries). The blue line follows the average energy for each orientation. The gray solid, dashed, and dotted lines are positioned at the global average, one standard deviation less than the global average, and two standard deviations less than the global average, respectively. (For interpretation of the references to color in this figure legend, the reader is referred to the web version of this article.)

and dotted gray lines are located at one and two standard deviations less than the average minimum energy. The average minimum energy over all orientations for Ni (Al) was  $0.743 \text{ J}/\text{m}^2 \pm 0.214 \text{ J}/\text{m}^2$  ( $0.297 \text{ J}/\text{m}^2 \pm 0.076 \text{ J}/\text{m}^2$ ). The average minimum energy over all orientations for Fe (Mo) was  $0.646 \text{ J}/\text{m}^2 \pm 0.235 \text{ J}/\text{m}^2$  ( $0.927 \text{ J}/\text{m}^2 \pm 0.332 \text{ J}/\text{m}^2$ ).

There is an overwhelming preponderance of  $\Sigma 3$  boundaries as the minimum energy boundary across substrate surface orientations for both crystal systems. There is an even stronger preference for  $\Sigma 3$  boundaries when considering only those below the average, or more

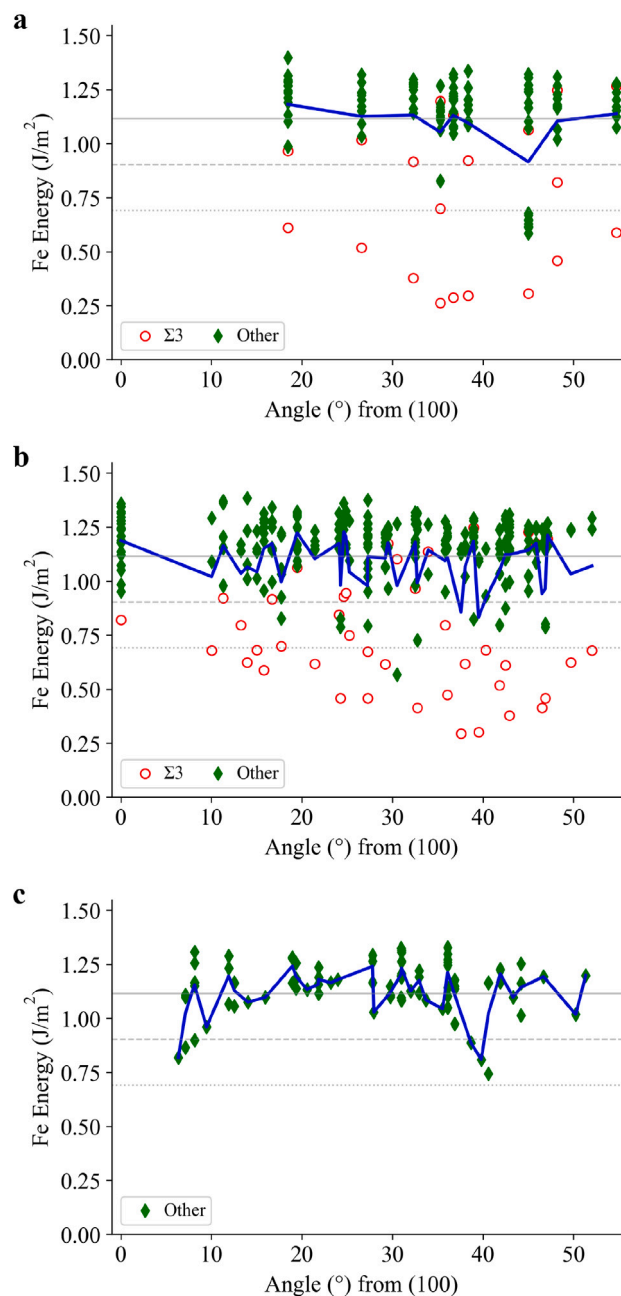


**Fig. 10.** Substrate (left grain boundary) orientations relative to the angle from (100) vs. grain boundary energy ( $\text{J}/\text{m}^2$ ) for *bcc* Fe. (a), (b), and (c), are respectively for orientations with two or more, one, and no  $\Sigma 3$  boundaries calculated. Red circles (green diamonds) indicate  $\Sigma 3$  boundaries (all other boundaries). The blue line follows the average energy for each orientation. The gray solid, dashed, and dotted lines are positioned at the global average, one standard deviation less than the global average, and two standard deviations less than the global average, respectively. (For interpretation of the references to color in this figure legend, the reader is referred to the web version of this article.)

than one standard deviation below the average of the minimum energy values. The only notable exceptions to  $\Sigma 3$  dominating the presence well below the average values in Figs. 11(a) and 11(b) (S4 and S5) are in *fcc*, a  $\Sigma 85$  and a  $\Sigma 11$ . The  $\Sigma 85$  is a twist boundary with a  $25.06^\circ$  rotation about  $\langle 100 \rangle$  and symmetric boundary plane normals of (100). The  $\Sigma 11$  is a tilt boundary with a  $50.48^\circ$  rotation about  $\langle 110 \rangle$  with symmetric boundary plane normals of (311). These will be discussed further below.

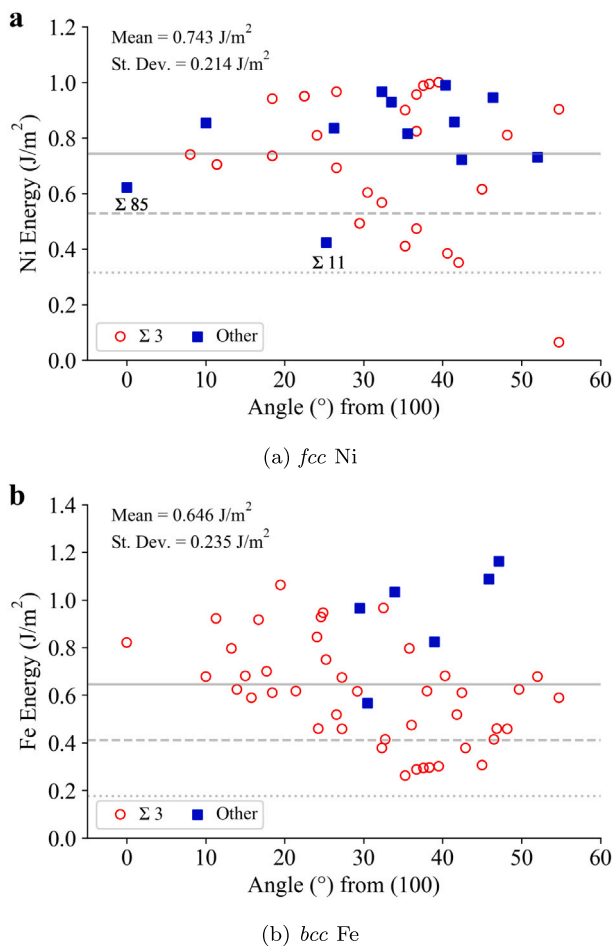


**Fig. 11.** Substrate (left grain boundary) orientations relative to the angle from (100) vs. grain boundary energy ( $\text{J/m}^2$ ) for the minimum value of a given orientation, for boundaries with 1 or more  $\Sigma 3$  boundaries calculated, for (a) *fcc* Ni and (b) *bcc* Fe. Red circles (blue squares) indicate orientations that are  $\Sigma 3$  (other  $\Sigma N$ ) boundaries. The gray solid, dashed, and dotted lines are positioned at the average of minimum energies, one standard deviation less than the average, and two standard deviations less than the average, respectively. (For interpretation of the references to color in this figure legend, the reader is referred to the web version of this article.)

### 3.5. Outliers to the generality of the $\Sigma 3$ OR

It is clear from the previous figures for *fcc* and *bcc* grain boundaries that the most likely lowest energy boundary will be a  $\Sigma 3$  boundary across habit plane orientation space. This is true even though not all of the  $\Sigma 3$  boundaries were computed for each orientation. For any given orientation, there may be multiple distinct  $\Sigma 3$  boundaries, and not all of these were computed. Not all  $\Sigma 3$  interfaces will be near the minimum energy for a given orientation, but one generally will be, as shown above. This can be seen in the plots where at least two  $\Sigma 3$  boundary energies were computed (Figs. 9a and Figs. 10a). In general, considering orientations where at least one  $\Sigma 3$  boundary was computed, the lowest  $\Sigma 3$  boundary energy is less than the global average over all orientations or *CSL* misorientations. Finally, for those orientations with no  $\Sigma 3$  boundary computed (see Figs. 9c and 10c), and even for some with only one or two, it may still be possible that a low-energy  $\Sigma 3$  boundary exists and should be calculated to further the hypothesis.

The main outliers to the preference of the  $\Sigma 3$  OR are the symmetric  $\Sigma 85(100)(100)$  and  $\Sigma 11(311)(311)$  Ni boundaries in Fig. 9b and 11(a). For both of these outliers, only one  $\Sigma 3$  had its grain boundary energy computed:  $0.810 \text{ J/m}^2$  and  $0.874 \text{ J/m}^2$ , respectively for the asymmetric

$\Sigma 3(100)(221)$  and the symmetric  $\Sigma 3(311)(311)$ . One can compute the distinct complementary planes for the  $\Sigma 3$  OR, as described in § S2 and shown in Table S1 for several substrate orientations. As shown in Table S1, there are no other  $\Sigma 3(100)$  interfaces, but there are two other  $\Sigma 3(311)$  interface possibilities that were not computed: (717) and (575). It is possible one of the latter may have lower energies than the  $\Sigma 3(311)(311)$  interface computed. One can see this occurs in the band of low-energy grain boundaries having (111) planes (at  $54.74^\circ$ ) with energies near  $0.4 \text{ J/m}^2$  and below two standard deviations from the global average (Fig. 9a). A  $\Sigma 3(111)(511)$  has a high energy ( $0.903 \text{ J/m}^2$ ) near one standard deviation below the global average, and well above the band of low-energy grain boundaries, but the  $\Sigma 3(111)(111)$  has the lowest energy over the entire space ( $0.064 \text{ J/m}^2$ ), considerably lower than the band observed (these are the only two planes for (111) substrates shown in Table S1).

The  $\Sigma 3(100)(221)$  and  $\Sigma 3(311)(311)$  values are similar to the higher energy  $\Sigma 3(111)(511)$ . To test whether a different  $\Sigma 3$  might have lower energies with a (311) substrate orientation, values of lower energy boundaries were computed using the grain boundary energy equation fitted by Abdeljawad et al. [41]:

$$\begin{aligned} \gamma_{gb}(\theta, \phi) = & \alpha_0 + \alpha_1 \cos(2\theta) + \alpha_2 \cos(4\theta) + \alpha_3 \cos(6\phi) \\ & + \alpha_4 \cos(6\phi) \cos(2\theta) + \alpha_5 \cos(6\phi) \cos(4\theta) + \alpha_6 \cos(12\phi) \end{aligned} \quad (1)$$

where  $\alpha_i$  ( $i = 0, \dots, 6$ ) are the fitted energy coefficients determined from atomistic data of  $\Sigma 3$  grain boundaries in Ni [28,29].  $\theta$  and  $\phi$  are the polar and azimuthal angles, measured from [111] and  $[11\bar{2}]$  crystal directions, respectively. Eq. (1) describes the minimum energies of  $\Sigma 3$  boundaries over all of orientation space. Using Eq. (1), the minimum  $\Sigma 3$  grain boundary energy was calculated to be  $0.856 \text{ J/m}^2$  and  $0.555 \text{ J/m}^2$ , for the  $\Sigma 3(100)$  and  $\Sigma 3(311)$ , respectively.

The fitted value for the  $\Sigma 3(100)(221)$  ( $0.856 \text{ J/m}^2$ ) is similar to the value in the computed data ( $0.810 \text{ J/m}^2$ ), indicating the relative difference between the fitted and computed data. There is only one  $\Sigma 3$  boundary for the (100) orientation of the substrate plane, it has a relatively high boundary energy (similar to other relatively high  $\Sigma 3$  boundaries), and there is a band of interfaces with similar energy, for which the lowest is the  $\Sigma 85(100)(100)$ . Thus, this orientation is an outlier to the general rule. Comparisons of the interfaces are shown in Fig. 12. The  $\Sigma 3(100)(221)$  (Fig. 12(a)) appears like all other  $\Sigma 3$  boundaries, with  $1/3$  of the atoms on (111) planes in coincidence at the interface. There is no obvious reason why the  $\Sigma 85(100)(100)$  interface is low in energy, as the interface plane has no obvious atomic coincidence, as viewed normal to the interface in Fig. 12(b).

The energy ( $0.555 \text{ J/m}^2$ ) of the  $\Sigma 3(311)(717)$  boundary (the (717) plane was determined using *GBTtoolbox* [42,43]) calculated from Eq. (1) is considerably lower than the value ( $0.874 \text{ J/m}^2$ ) for the  $\Sigma 3(311)(313)$  boundary computed in the original dataset. However, it is not as low as that of the  $\Sigma 11(311)(311)$  boundary computed there. Schematics of these two interfaces are given in Fig. 13. The  $\Sigma 3$  interface is similar to other  $\Sigma 3$  interfaces, having  $1/3$  of the atoms on (111) planes coincident at the interface. The  $\Sigma 11(311)(311)$  plane is a symmetric twin plane on which all atoms at the interface are coincident. This  $\Sigma 11(311)(311)$  is indeed a special interface and an outlier to the rule.

These results (and the computations shown in Table S1) indicate that multiple  $\Sigma 3$  boundaries exist for many of the orientations considered here, and that the lowest energy value may not have been computed. Nevertheless, the preponderance of  $\Sigma 3$  as the lowest energy for any orientation, and its preponderance in the outlier low values for almost all orientations, the lack of any outliers in *bcc*, and the existence of only two outliers in *fcc* are all consistent with  $\Sigma 3$  as the preferred OR at grain boundaries in *fcc* and *bcc* structures. The few outlier boundaries are simply specific exceptions to the general rule, though only one has an obvious reason it is an outlier.

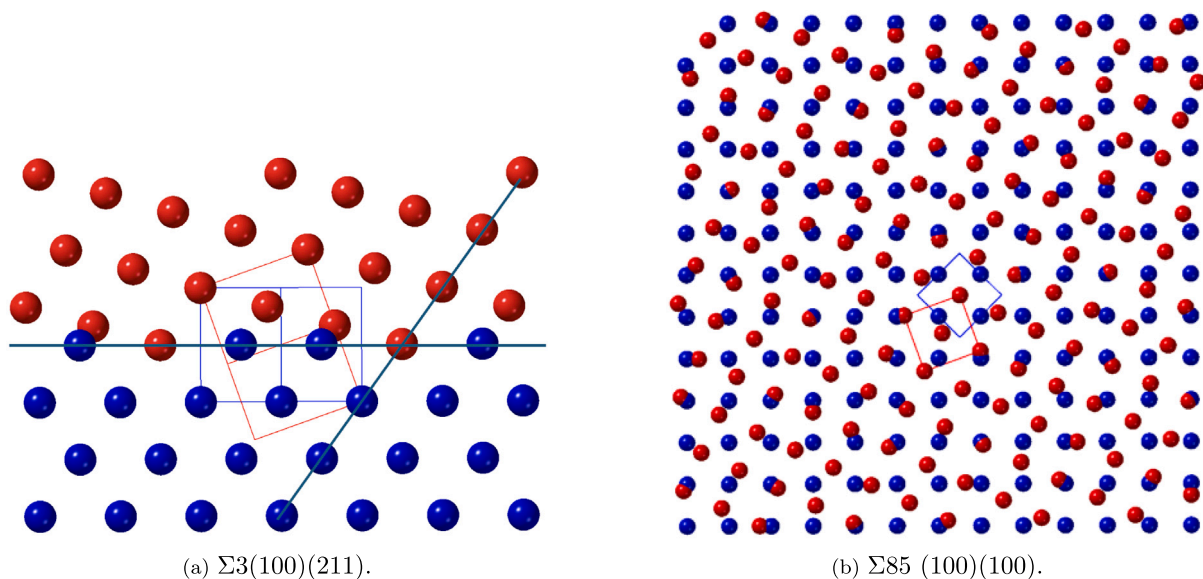


**Fig. 12.** Schematic interfaces with a (100) substrate plane (blue atoms). In (a), the interface plane is marked as the horizontal line and the (111) plane is marked as the slanted line. The film (red atoms) has a  $\Sigma 3$  misorientation and a (211) plane.  $1/3$  of the atoms on the (111) planes are coincident at the interface. In (b), the interface is viewed in the direction of the normal and the film (red atoms) has a  $\Sigma 85$  misorientation and a (100) plane. Only  $1/85$  lattice sites at the interface will be coincident. Unit cells of each are shown in each, with a  $\langle 1\bar{1}0 \rangle$  and  $\langle 100 \rangle$  pointing into the page respectively for (a) and (b). (For interpretation of the references to color in this figure legend, the reader is referred to the web version of this article.)

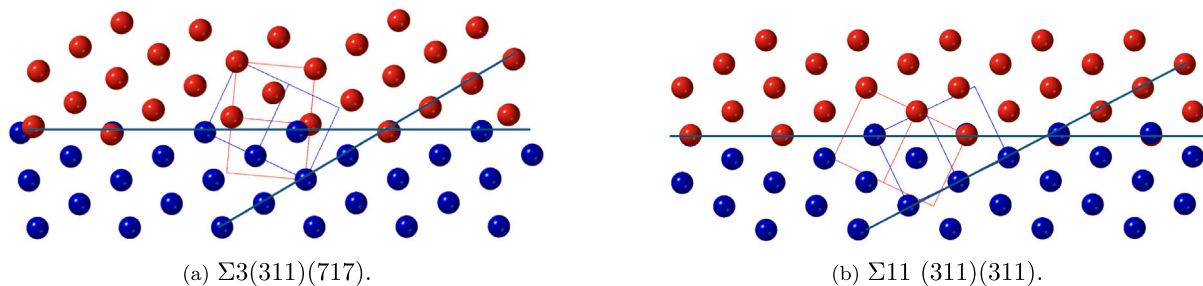


**Fig. 13.** Schematic interfaces with a (311) substrate plane (blue atoms). The interface plane is marked as the horizontal line and the (111) plane is marked as the slanted line. In (a) the film (red atoms) has a  $\Sigma 3$  misorientation and a (717) plane. In (b) the film (red atoms) has a  $\Sigma 11$  misorientation and a (311) plane. The latter (former) has all ( $1/3$ ) of the atoms on the (111) planes coincident at the interface. Unit cells of each are shown, with a  $\langle 1\bar{1}0 \rangle$  pointing into the page. (For interpretation of the references to color in this figure legend, the reader is referred to the web version of this article.)

## 4. Discussion

### 4.1. Preferred ORs at interfaces of crystals

Evidence was presented that supports the existence of general, preferred orientation relationships (ORs) at interfaces of crystals, regardless of the nature of the interface plane and whether considering hetero-epitaxial interfaces or grain boundaries. Reviewing observations from high-throughput thin-film growth, the preferred OR for many non-isostructural oxide film–substrate pairs is the eutactic OR: the one that aligns the nearly closed-packed plane and direction in 3D (which was shown herein to be a type of  $\Sigma 3$  OR). This has been observed over all of substrate orientation space for a variety of nearly close-packed materials. Because orientations are selected during epitaxial growth owing to them being the lowest in energy, these observations imply that the eutactic alignment is one that minimizes the interface energy between substrate and film, regardless of interface plane. That the 3D orientation determines epitaxial ORs in CSE differs from the common rationalization focusing on 2D geometry matching at interfaces.

The preferred OR hypothesis was further tested using data from the grain boundary community. Two large datasets of computed grain boundary energies were revisited and sorted using a conceptual combinatorial substrate epitaxy (CSE) experiment. For 388 *fcc* and 408 *bcc*

grain boundaries in metals, it was found that the  $\Sigma 3$  OR leads to the lowest grain boundary energy compared to other CSL ORs in the data set, regardless of a given interface plane orientation, with two outliers in the *fcc* data. In general, selecting the lowest-energy interface is not kinetically accessible during grain growth, and therefore this preferred orientation at grain boundaries is not experimentally reported. Nevertheless, the computed grain boundary energies support a strong probability that the lowest-energy interface for a given grain boundary plane corresponds a  $\Sigma 3$  OR.

These observations address the fundamental question raised in the Introduction: Is there a general preferred orientation relationship between crystals at interfaces? The answer is yes. Simple general 3D ORs are preferred at the interfaces of crystals, specifically:

(1) the eutactic OR in oxide heteroepitaxy, which is a type of  $\Sigma 3$  OR, and

(2) the  $\Sigma 3$  OR at grain boundaries in *fcc* and *bcc*.

More specifically, this means that a single 3D OR leads to the lowest energy interface for any orientation of the interface plane (outliers notwithstanding).

### 4.2. Structural variability at interfaces

The existence of a general preferred OR at interfaces describes, at the highest level, a global preference. It is expected that many

specifics will vary based on details of the structure of exact interfaces, especially considering strain and composition. For example, enormous subtle details of basic cube-on-cube epitaxy have been characterized in the literature, including unit-cell strain, bonding variations, electronic transitions, misfit dislocations or disconnections, etc [3,44–47]. Such details have important implications for properties, even leading to emergent bulk or interface properties [44,45,48,49]. One also anticipates structural variations to occur at general interfaces described here, including small rotations away from the precise alignment of the preferred OR. In fact, the observable angular variations (usually below 5°) around the precise angular expectations of the eutactic OR in CSE are likely caused by these specific differences. Nevertheless, the overall orientation is consistent with the eutactic one, and the small rotational differences may arise from second-order terms further lowering the energy through small rotations (or other strains and structural relaxations).

#### 4.3. Minimum energy values and outliers

One of the interesting observations in the computed grain boundary data is that the value of the lowest energy  $\Sigma 3$  boundary is not always quantitatively low. The average minimum energy over all orientations for *fcc* Ni (Al) was 0.743 (0.297) and for *bcc* Fe (Mo) was 0.646 (0.927) J/m<sup>2</sup>, while the average overall grain boundary energies for *fcc* Ni (Al) was 1.09 (0.42) and for *bcc* Fe (Mo) was 1.11 (1.59) J/m<sup>2</sup>. Thus, the average lowest energy was 68.2 (70.7)% and 58.2 (58.3)% of the average overall grain boundary energy, for Ni (Al) and Fe (Mo), respectively. (The standard deviations on the average values are approximately 20% of the global average for any system.)

The lowest  $\Sigma 3$  energy corresponds to the coherent twin in both systems: the (111) symmetric twist in *fcc* and the (211) symmetric tilt boundary in *bcc*, respectively 54.7° and 35.2° from the (100). The energy of the  $\Sigma 3$  boundaries generally increases as one rotates away from the coherent twin towards the (100). The lowest values reported (excluding the  $\Sigma 3$  coherent twin in *fcc*) are  $\approx 32$  (40)% and 23 (25)% of the average overall grain boundary energy, for Ni (Al) and Fe (Mo), respectively. Thus, the minimum energy values essentially range from  $\approx 30$  to 70% and 25 to 60% of the average grain boundary values, for *fcc* and *bcc* respectively, with values generally increasing with angle away from the coherent twin.

As a result, it should not be surprising that some boundaries with other ORs may have lower energies. In this work, only the  $\Sigma 11(311)(311)$  and  $\Sigma 85(100)(100)$  boundaries in *fcc* metals fit this description. Even considering an empirical fit to the computed data, the  $\Sigma 11$  and  $\Sigma 85$  boundaries remain lower than competitive  $\Sigma 3$  boundaries.  $\Sigma 11$  and  $\Sigma 85$  are not low  $\Sigma N$  values, and they are somewhat hard to predict as outliers, especially since their energies are not extraordinarily low (with energies of 0.424 and 0.622 J/m<sup>2</sup>, respectively, or 39% and 57% of the average grain boundary energy). These planes are respectively 35.3° and 54.7° from the coherent twin. The  $\Sigma 11$  can be rationalized as a structural low energy boundary, being a twin boundary with high atom coincidence at the interface; the  $\Sigma 85$  cannot be. These outliers indicate that circumstances will arise where other low energy ORs exist, likely as one rotates significantly from the coherent plane and the  $\Sigma 3$  energy increases. There are still somewhat similarly low energy  $\Sigma 3$  competing near the lowest energy for the given habit plane, just not as the minimum energy. Similarly, when the preferred OR is the  $\Sigma 3$ , there can be other ORs with just slightly higher energies too, such as the band of low energy ORs in Ni at the (111) plane (54.7° from (100) with other interface planes than the symmetric (111)) or in Fe at the (110) plane (45° from (100)). In kinetically constrained situations, other low-energy ORs may also be accessible instead of only the lowest-energy one.

#### 4.4. Epitaxy and computed energies

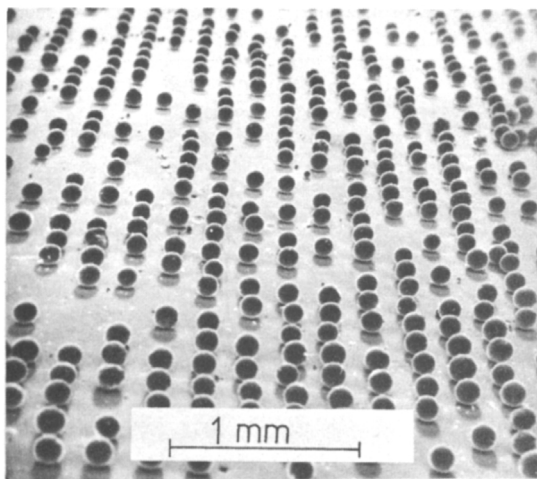
The alignment of eutactic planes and directions in oxide epitaxy results in the eutactic OR. The eutactic OR is also a type of  $\Sigma 3$  OR (Fig. 4), though not identical to the  $\Sigma 3$  OR for *fcc*, considering the repeat periods for coincidence. When the eutactic plane is the habit plane of the interface, the interface is closest to coherency in epitaxy of non-isostructural systems, and the OR is similar to the coherent twin  $\Sigma 3$  OR. If the analogy can be extended, one expects the lowest energy for the possibly coherent eutactic OR, with the energy increasing in angle as one moves away from this orientation. CSE observations generally support this, where the destabilization of stable close-packed oxides is largest the farthest one rotates away from the coherent interface [26,37]. Based on the behavior of  $\Sigma 3$  grain boundary energies, one interpretation is that the interface energy increases with the rotation angle away from the coherent interface, destabilizing the stable phase based on the interface energy.

In general, computational studies of thin film interfaces are sparse, focus on narrow and specific cases, usually focus on strain and physical properties, and are almost always coherent interfaces [50–55]. Recently, the authors have been developing a methodology called computationally guided epitaxial synthesis (CGES) [54–56], in which density functional theory (DFT) computations are used to estimate the energetics of bulk materials, strained materials, and coherent interfaces of bulk metastable structures. CGES studies have been reported for relative polymorph stability in dioxides  $BO_2$  [56], for rutile/anatase  $TiO_2$  films on 3D (Sr,Ba) $TiO_3$  substrates [54], and for 3C and 4H (Sr,Ba) $MnO_3$  on 3C (Sr,Ba) $TiO_3$  [55]. In the current CGES models, only approximate values of incoherent interfaces of bulk stable phases are used. For all cases of expected incoherent interfaces, the interface energy was approximated as 1 J/m<sup>2</sup> [54], which approximates the interfacial energies of oxides [11,57–59].

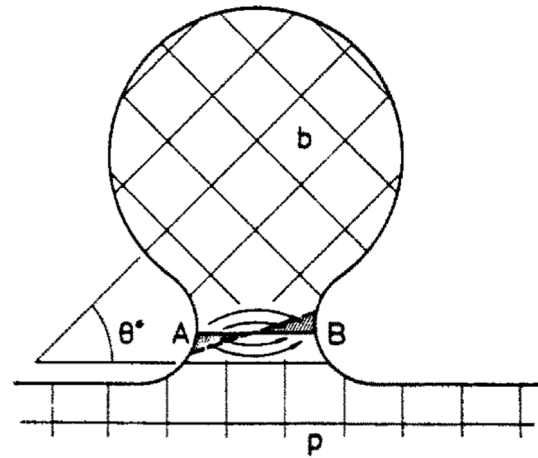
Using the computations for metals re-described herein, one can reconsider the value of the energy for CGES models. For the metal systems described here, the average incoherent interface is indeed on the order of 1 J/m<sup>2</sup>, but varies depending on the material system. As discussed before, the average of the lowest energy value for incoherent interfaces for a given orientation are  $\approx 70$  and 60% of the average grain boundary energy (though a function of orientation), for *fcc* and *bcc* respectively. This forms a baseline for comparison of other systems. For  $SrTiO_3$ , a cubic close packed oxide similar to *fcc*, grain boundary energies are  $\approx 1.0$  J/m<sup>2</sup>, depending on the grain boundary plane orientation [57]. Thus, the energy of a preferred grain boundary OR would average around 0.7 J/m<sup>2</sup>, assuming oxides behave similarly to the metals. The range of minimum incoherent interface energies is likely to be from 0.33 to 1.0 J/m<sup>2</sup>, and a function of orientation. When comparing to the incoherent interface energy in epitaxy, this range is sufficiently lower than the 1 J/m<sup>2</sup> estimation to matter for phase stability (by a factor of 2 or 3 in some cases). While the exact interface energies may differ between oxides and metals, this seems to be a reasonable starting point for estimates. Thus, it is important to develop approaches to estimate interface energies in epitaxial systems as done here for metals. Of course, having methods to compute incoherent interface energies would help address this hypothesis, and improve CGES significantly too.

#### 4.5. Sphere-on-plate interface comparisons

The fashion in which typical grain boundaries form differs significantly from how an epitaxial film forms. The orientations of the two grains that form a grain boundary are essentially fixed; they are kinetically hindered and are interconnected with other neighboring grains such that they cannot re-orient simultaneously to satisfy the preferred orientation at all interfaces. Thus, there is very little physical evidence that a preferred misorientation exists at general grain boundaries, in contrast to the CSE observations for epitaxial films.



(a) Single crystal Cu microspheres on a plate of Cu.



(b) Schematic cross section of one sphere (*b*) on a plate.

**Fig. 14.** (a) A scanning electron microscope image of many single crystal copper microspheres on a single crystal Cu plate. (b) A schematic cross-section of one sphere (*b*) on a plate (*p*) with grain boundary *AB* between them and a misorientation angle  $\theta$  between structures. Arrows indicate diffusive flux that causes rotation of the sphere. Source: Both are reproduced from [61] with permission.

So called sphere-on-plate grain boundary experiments [60–68] address the same question as does the hypothetical CSE experiments described herein. In these high-throughput experiments, a large number of single-crystal micro-spheres of a material (often *fcc*) are dispersed onto a macro-scale single-crystal plate (often of the same composition) with a single surface orientation. An example of *fcc* Cu microspheres dispersed on a Cu single crystal is shown in Fig. 14(a) [61]. The system is annealed to close to the melting temperature and the spheres rotate and sinter to the flat substrate. The rotations are driven by grain boundary energy gradients, and the spheres move towards minima positions in energy space forming a grain boundary that is generally parallel to the original surface (when interface energies drive the outcomes and local equilibrium is achieved; in some cases the boundary can be inclined and others it can be faceted at the meso-scale). A proposed mechanism of rotation for a single sphere is shown in Fig. 14(b) [61]. Systems investigated include *fcc* materials Cu [61,63–68], Ag [62,65], and Ni [64] with a (100) [61,62,64–67], (110) [61–63,65], or (111) [61,62,65,67,68] surface plane (and some alloys [62,64,67] and heterophase boundaries [69–71] that are similar to CSE investigations). As the annealing temperature is increased towards the melting temperature, the number and types of grain boundaries observed decreases towards (presumably) the lowest energy arrangement(s) [63]. While the rotation mechanisms are complex, which hinders a complete understanding of why certain orientations are found in the final distributions, it is clear that a small number of low  $\Sigma$  value CSL orientations dominate the final distributions at the highest temperatures.

On (100), (110), and (111) oriented *fcc* single crystals,  $\Sigma 3$  ORs are always the most frequently observed OR. However, more than one OR is usually observed, including more than one  $\Sigma 3$  OR. On the (111) surface, the coherent twin symmetric  $\Sigma 3$  OR is globally the lowest energy boundary ( $0.064 \text{ J/m}^2$  for Ni), but it is not uniquely observed nor is it always the most observed  $\Sigma 3$  OR for Cu or Ag [61,66,67]. The asymmetric  $\Sigma 3(111)(511)$  OR is one of the highest energies in the computed dataset for (111) surfaces (at  $0.903 \text{ J/m}^2$  for Ni), but it is also observed [65,66]. These clearly indicate that the sphere-on-plate experiments do not lead to global minima, but to local minima in energy space, and these minima are not necessarily extraordinarily low in energy.

On (110) single crystals, the asymmetric  $\Sigma 3(110)(411)$  OR is the lowest energy for Ni at  $0.615 \text{ J/m}^2$ , while the symmetric  $\Sigma 3(110)(110)$  OR energy is  $1.005 \text{ J/m}^2$ . The most frequent observation for *fcc* sphere-on-plate experiments is sometimes the asymmetric  $\Sigma 3(110)(411)$

OR [65] but other times it is the symmetric  $\Sigma 3(110)(110)$  OR [61]. On (100) single crystals, the most observed OR is the  $\Sigma 3(100)(221)$  [61, 64,67]. The  $\Sigma 85(100)(100)$  has not been reported in any of the sphere-on-plate experiments, although it is the lowest energy at  $0.622 \text{ J/m}^2$  for Ni. The energy of Ni  $\Sigma 3(100)(221)$  is significantly higher at  $0.81 \text{ J/m}^2$ . On both substrate orientations (110) and (100), many other orientations are also observed, again indicating that sphere-on-plate experiments produce local minima in energy space, and these minima are not necessarily extraordinarily low in energy.

The deviations between the sphere-on-plate observations and the computed dataset low-energy ORs appear to arise from kinetic effects, as described in the literature discussed [60–68]. This appears to be most relevant for the (100) surfaces where the low-energy but high- $\Sigma$ -value OR  $\Sigma 85(100)(100)$  has never been reported. Thus, the sphere-on-plate experiments indicate that the  $\Sigma 3$  boundaries are significant energy minima across OR phase space, regardless of low-index orientation of the single crystal, but also that these are often kinetically preferred orientations as well.

Some sphere-on-plate experiments focused on hetero-phase interfaces [69–71], mostly *fcc* metals on ionic rock-salt crystals, which are analogous to CSE experiments. Most observations agree with the conclusions made above for grain boundaries from sphere-on-plate experiments. Furthermore, these heterophase experiments agree with the CSE observations that the eutactic OR is one of the lowest energy ORs. The preferred ORs in the hetero-phase experiments were the set described by the so-called the lock-in model [69]: those ORs which aligned the close-packed rows of atoms (the eutactic directions). CSE experiments suggest that the eutactic OR is the lowest energy of all such lock-in ORs; kinetics prevent sphere-on-plate experiments from finding the global minimum [69–71]. In CSE experiments, films are crystallized from the vapor phase at rates that allow for the selection of the lowest energy OR [23–26,31–37]. Kinetic effects also impact CSE observations, but these can be somewhat manipulated by controlling growth rates and temperature. However, it cannot be ruled out that preferred kinetics for forming the eutactic OR increases the frequency of its observation, similar to the sphere-on-plate observations for  $\Sigma 3$  ORs for *fcc* grain boundaries. Combining the thermodynamic support for the  $\Sigma 3$  presented herein, with the kinetic support from the sphere-on-plate observations, both appear to work in favor of accessing the preferred OR in CSE. A small number of other orientations (though still the minority of ORs) were reported for hematite  $\text{Fe}_2\text{O}_3$  deposited on

perovskite SrTiO<sub>3</sub> (100) single crystals under conditions that supported eutactic OR on all orientations of polycrystalline SrTiO<sub>3</sub> [24]. This observation indicates that kinetic effects are also important in CSE, but the majority of observations on the single crystal and the overwhelming observation of the eutactic OR on polycrystals implies thermodynamics dominate the OR selection.

## 5. Conclusions

The existence of a preferred orientation at crystalline interfaces was reviewed for epitaxial oxide films and demonstrated for grain boundaries. A simple general descriptor of the preferred epitaxial OR is the alignment of the eutactic (nearly close-packed) planes and directions, called the eutactic OR and shown to be a type of  $\Sigma 3$  CSL OR. This is experimentally found in high-throughput epitaxial investigations, called combinatorial substrate epitaxy (CSE), and rationalized because many crystal structures can be described by eutaxy. A general preferred OR was demonstrated for grain boundaries using previously reported computed grain boundary energies in *fcc* (388 boundaries) and *bcc* (408 boundaries) metals. Based on low-energy outliers in the grain boundary populations, it is shown that the  $\Sigma 3$  coincident site lattice (CSL) misorientation is the preferred OR for both families of metals, regardless of interface orientation. While the overall energy still varies as a function of grain boundary plane and misorientation, and the lowest energy grain boundary value varies as a function of habit plane orientation, a  $\Sigma 3$  OR (or misorientation) is almost always the OR with the lowest energy at a given orientation. This evidence unites the epitaxial interface community with the grain boundary community, indicating that the 3D OR is important in determining the energy of a general interface, given a fixed orientation of one habit plane for the interface. All of these observations are consistent with the existence of a single preferred OR (or misorientation) at interfaces of crystals: for all systems investigated here, the preferred OR is a  $\Sigma 3$  OR.

## CRedit authorship contribution statement

**Catherine Zhou:** Writing – original draft, Visualization, Validation, Software, Resources, Methodology, Investigation, Formal analysis, Data curation, Conceptualization. **Gregory S. Rohrer:** Writing – review & editing, Supervision, Resources, Project administration, Methodology, Funding acquisition, Data curation, Conceptualization. **Paul A. Salvador:** Writing – original draft, Visualization, Validation, Supervision, Project administration, Methodology, Funding acquisition, Formal analysis, Conceptualization.

## Declaration of competing interest

The authors declare that they have no known competing financial interests or personal relationships that could have appeared to influence the work reported in this paper.

## Acknowledgments

C.Z., P.A.S., and G.S.R. acknowledge the support of the National Science Foundation, USA [DMR-1609355].

## Appendix A. Supplemental information

Supplementary material related to this article can be found online at <https://doi.org/10.1016/j.mtadv.2025.100580>. Complementary figures to Figs. 8–11 are given in the supplementary information, focusing on a different system for Fig. 8, or a different material for Figs. 9–11. There is also a brief section discussing how to find film planar matches to a given substrate orientation for the grain boundary  $\Sigma 3$  OR.

## Data availability

Data will be made available on request.

## References

- [1] W.K. Burton, N. Cabrera, F.C. Frank, N.F. Mott, The growth of crystals and the equilibrium structure of their surfaces, *Philos. Trans. R. Soc. Lond. Ser. A, Math. Phys. Sci.* 243 (866) (1951) 299–358, <http://dx.doi.org/10.1098/rsta.1951.0006>.
- [2] Y.-S. Jun, D. Kim, C.W. Neil, Heterogeneous nucleation and growth of nanoparticles at environmental interfaces, *Acc. Chem. Res.* 49 (9) (2016) 1681–1690, <http://dx.doi.org/10.1021/acs.accounts.6b00208>.
- [3] M.A. Herman, W. Richter, H. Sitter, *Epitaxy: Physical Principles and Technical Implementation*, Springer, Oxford, 2004.
- [4] J.P. Hirth, The influence of grain boundaries on mechanical properties, *Met. Trans.* 3 (12) (1972) 3047–3067, <http://dx.doi.org/10.1007/BF02661312>.
- [5] A.P. Sutton, R.W. Balluffi, *Interfaces in Crystalline Materials*, Clarendon Press, Oxford, 1995.
- [6] A. Gozar, G. Logvenov, L.F. Kourkoutis, A.T. Bollinger, L.A. Giannuzzi, D.A. Muller, I. Bozovic, High-temperature interface superconductivity between metallic and insulating copper oxides, *Nature* 455 (7214) (2008) 782–785, <http://dx.doi.org/10.1038/nature07293>.
- [7] H.Y. Hwang, Y. Iwasa, M. Kawasaki, B. Keimer, N. Nagaosa, Y. Tokura, Emergent phenomena at oxide interfaces, *Nat. Mater.* 11 (2) (2012) 103–113, <http://dx.doi.org/10.1038/nmat3223>.
- [8] A. Gozar, I. Bozovic, High temperature interface superconductivity, *Phys. C: Supercond. Appl.* 521–522 (2016) 38–49, <http://dx.doi.org/10.1016/j.physc.2016.01.003>.
- [9] M. Ohring, Chapter 8 - epitaxy, in: M. Ohring (Ed.), *Materials Science of Thin Films*, second ed., Academic Press, San Diego, 2002, pp. 417–494, <http://dx.doi.org/10.1016/B978-012524975-1/50011-2>.
- [10] C.J. Palmstrom, Epitaxy of dissimilar materials, *Annu. Rev. Mater. Sci.* 25 (1) (1995) 389–415, <http://dx.doi.org/10.1146/annurev.ms.25.080195.002133>.
- [11] O.Y. Gorbenko, S.V. Samoilenkov, I.E. Graboy, A.R. Kaul, Epitaxial stabilization of oxides in thin films, *Chem. Mater.* 14 (10) (2002) 4026–4043, <http://dx.doi.org/10.1021/cm021111v>.
- [12] J. Narayan, B.C. Larson, Domain epitaxy: A unified paradigm for thin film growth, *J. Appl. Phys.* 93 (1) (2003) 278–285, <http://dx.doi.org/10.1063/1.1528301>.
- [13] R.Z. Valiev, V.Y. Gertsman, O.A. Kaibyshev, Grain boundary structure and properties under external influences, *Phys. Status Solidi (A)* 97 (1) (1986) 11–56, <http://dx.doi.org/10.1002/pssa.2210970102>.
- [14] G.S. Rohrer, Measuring and interpreting the structure of grain-boundary networks, *J. Am. Ceram. Soc.* 94 (3) (2011) 633–646, <http://dx.doi.org/10.1111/j.1551-2916.2011.04384.x>.
- [15] T. Watanabe, Grain boundary engineering: historical perspective and future prospects, *J. Mater. Sci.* 46 (12) (2011) 4095–4115, <http://dx.doi.org/10.1007/s10853-011-5393-z>.
- [16] P.R. Cantwell, M. Tang, S.J. Dillon, J. Luo, G.S. Rohrer, M.P. Harmer, Grain boundary complexions, *Acta Mater.* 62 (2014) 1–48, <http://dx.doi.org/10.1016/j.actamat.2013.07.037>.
- [17] M. Ohring (Ed.), *Materials Science of Thin Films (Second Edition)*, second ed., Academic Press, San Diego, 2002, p. 794, <http://dx.doi.org/10.1016/B978-0-12-524975-1.X5000-9>.
- [18] G. Gilmer, H. Huang, C. Roland, Thin film deposition: fundamentals and modeling, *Comput. Mater. Sci.* 12 (4) (1998) 354–380, [http://dx.doi.org/10.1016/S0927-0256\(98\)00022-6](http://dx.doi.org/10.1016/S0927-0256(98)00022-6).
- [19] R. Kobayashi, J. Warren, W. Carter, Vector-valued phase field model for crystallization and grain boundary formation, *Phys. D: Nonlinear Phenom.* 119 (3) (1998) 415–423, [http://dx.doi.org/10.1016/S0167-2789\(98\)00026-8](http://dx.doi.org/10.1016/S0167-2789(98)00026-8).
- [20] J. Han, S.L. Thomas, D.J. Srolovitz, Grain-boundary kinetics: A unified approach, *Prog. Mater. Sci.* 98 (2018) 386–476, <http://dx.doi.org/10.1016/j.pmatsci.2018.05.004>.
- [21] Z. Xu, C.M. Hefferan, S.F. Li, J. Lind, R.M. Suter, F. Abdeljawad, G.S. Rohrer, Energy dissipation by grain boundary replacement during grain growth, *Scr. Mater.* 230 (2023) 115405, <http://dx.doi.org/10.1016/j.scriptamat.2023.115405>.
- [22] G.S. Rohrer, D.M. Saylor, B. El Dasher, B.L. Adams, A.D. Rollett, P. Wynblatt, The distribution of internal interfaces in polycrystals, *Int. J. Mater. Res.* 95 (4) (2004) 197–214, <http://dx.doi.org/10.3139/jjmr-2004-0043>.
- [23] C. Zhou, M. De Graef, B. Dabrowski, G.S. Rohrer, P.A. Salvador, Combinatorial substrate epitaxy investigation of polytypic growth of AEMnO<sub>3</sub> (AE=Ca, Sr), *J. Am. Ceram. Soc.* 103 (3) (2020) 2225–2234, <http://dx.doi.org/10.1111/jace.16867>.
- [24] A.M. Schultz, Y. Zhu, S.A. Bojarski, G.S. Rohrer, P.A. Salvador, Eutaxial growth of hematite Fe<sub>2</sub>O<sub>3</sub> films on perovskite SrTiO<sub>3</sub> polycrystalline substrates, *Thin Solid Films* 548 (2013) 220–224, <http://dx.doi.org/10.1016/j.tsf.2013.09.073>.

- [25] N.V. Burbure, P.A. Salvador, G.S. Rohrer, Orientation and phase relationships between titania films and polycrystalline BaTiO<sub>3</sub> substrates as determined by electron backscatter diffraction mapping, *J. Am. Ceram. Soc.* 93 (9) (2010) 2530–2533, <http://dx.doi.org/10.1111/j.1551-2916.2010.03878.x>.
- [26] Y. Zhang, A.M. Schultz, L. Li, H. Chien, P.A. Salvador, G.S. Rohrer, Combinatorial substrate epitaxy: A high-throughput method for determining phase and orientation relationships and its application to BiFeO<sub>3</sub>/TiO<sub>2</sub> heterostructures, *Acta Mater.* 60 (19) (2012) 6486–6493, <http://dx.doi.org/10.1016/j.actamat.2012.07.060>.
- [27] M. O'Keefe, On the arrangements of ions in crystals, *Acta Crystallogr.* A33 (6) (1977) 924–927, <http://dx.doi.org/10.1107/S056773947700223X>.
- [28] D.L. Olmsted, S.M. Foiles, E.A. Holm, Survey of computed grain boundary properties in face-centered cubic metals: I. Grain boundary energy, *Acta Mater.* 57 (13) (2009) 3694–3703, <http://dx.doi.org/10.1016/j.actamat.2009.04.007>.
- [29] D.L. Olmsted, E.A. Holm, S.M. Foiles, Survey of computed grain boundary properties in face-centered cubic metals—II: Grain boundary mobility, *Acta Mater.* 57 (13) (2009) 3704–3713, <http://dx.doi.org/10.1016/j.actamat.2009.04.015>.
- [30] S. Ratanaphan, D.L. Olmsted, V.V. Bulatov, E.A. Holm, A.D. Rollett, G.S. Rohrer, Grain boundary energies in body-centered cubic metals, *Acta Mater.* 88 (2015) 346–354, <http://dx.doi.org/10.1016/j.actamat.2015.01.069>.
- [31] S. Havelia, S. Wang, K.R. Balasubramaniam, A.M. Schultz, G.S. Rohrer, P.A. Salvador, Combinatorial substrate epitaxy: A new approach to growth of complex metastable compounds, *CrystEngComm* 15 (27) (2013) 5434–5441, <http://dx.doi.org/10.1039/C3CE40469B>.
- [32] D. Pravarthana, M. Trassin, J. Haw Chu, M. Lacotte, A. David, R. Ramesh, P.A. Salvador, W. Prellier, BiFeO<sub>3</sub>/La<sub>0.7</sub>Sr<sub>0.3</sub>MnO<sub>3</sub> heterostructures deposited on spark plasma sintered LaAlO<sub>3</sub> substrates, *Appl. Phys. Lett.* 104 (8) (2014) 082914, <http://dx.doi.org/10.1063/1.4867021>.
- [33] M. Lacotte, A. David, D. Pravarthana, C. Grygiel, G.S. Rohrer, P.A. Salvador, M. Velazquez, R. de Kloe, W. Prellier, Growth of Ca<sub>2</sub>MnO<sub>4</sub> Ruddlesden-Popper structured thin films using combinatorial substrate epitaxy, *J. Appl. Phys.* 116 (24) (2014) 245303, <http://dx.doi.org/10.1063/1.4905012>.
- [34] M. Lacotte, A. David, G.S. Rohrer, P.A. Salvador, W. Prellier, Preferential orientation relationships in Ca<sub>2</sub>MnO<sub>4</sub> Ruddlesden-Popper thin films, *J. Appl. Phys.* 118 (4) (2015) 045306, <http://dx.doi.org/10.1063/1.4927518>.
- [35] D. Pravarthana, O.I. Lebedev, A. David, A. Fouchet, M. Trassin, G.S. Rohrer, P.A. Salvador, W. Prellier, Metastable monoclinic [110] layered perovskite Dy<sub>2</sub>Ti<sub>2</sub>O<sub>7</sub> thin films for ferroelectric applications, *RSC Adv.* 9 (35) (2019) 19895–19904, <http://dx.doi.org/10.1039/c9ra04554f>.
- [36] J. Wittkamper, Z. Xu, B. Kombariah, F. Ram, M. De Graef, J.R. Kitchin, G.S. Rohrer, P.A. Salvador, Competitive growth of scrutinyite (α-PbO<sub>2</sub>) and rutile polymorphs of SnO<sub>2</sub> on all orientations of columbite CoNb<sub>2</sub>O<sub>6</sub> substrates, *Cryst. Growth & Des.* 17 (7) (2017) 3929–3939, <http://dx.doi.org/10.1021/acs.cgd.7b00569>.
- [37] C. Zhou, G.S. Rohrer, M. De Graef, P.A. Salvador, Epitaxial phase stability of SrMnO<sub>3-x</sub> films on polycrystalline perovskite substrates, *Cryst. Growth & Des.* 21 (8) (2021) 4547–4555, <http://dx.doi.org/10.1021/ACS.CGD.1C00429>.
- [38] F.J. Wong, S. Ramanathan, Nonisostructural complex oxide heteroepitaxy, *J. Vac. Sci. Technol. A* 32 (4) (2014) 040801, <http://dx.doi.org/10.1116/1.4879695>.
- [39] S. Ranganathan, On the geometry of coincidence-site lattices, *Acta Crystallogr.* 21 (2) (1966) 197–199, <http://dx.doi.org/10.1107/S0365110X66002615>.
- [40] A. Brokman, R. Balluffi, Coincidence lattice model for the structure and energy of grain boundaries, *Acta Metall.* 29 (10) (1981) 1703–1719, [http://dx.doi.org/10.1016/0001-6160\(81\)90005-5](http://dx.doi.org/10.1016/0001-6160(81)90005-5).
- [41] F. Abdeljawad, S.M. Foiles, A.P. Moore, A.R. Hinkle, C.M. Barr, N.M. Heckman, K. Hattar, B.L. Boyce, The role of the interface stiffness tensor on grain boundary dynamics, *Acta Mater.* 158 (2018) 440–453, <http://dx.doi.org/10.1016/j.actamat.2018.06.025>.
- [42] K. Glowinski, GBToolbox, 2022, URL <https://github.com/kglowins/gbtoolbox-legacy>. (Accessed 2022).
- [43] A. Morawiec, K. Glowinski, On “macroscopic” characterization of mixed grain boundaries, *Acta Mater.* 61 (15) (2013) 5756–5767, <http://dx.doi.org/10.1016/j.actamat.2013.06.019>.
- [44] D.G. Schlom, L.-Q. Chen, X. Pan, A. Schmehl, M.A. Zurbuchen, A thin film approach to engineering functionality into oxides, *J. Am. Ceram. Soc.* 91 (8) (2008) 2429–2454, <http://dx.doi.org/10.1111/j.1551-2916.2008.02556.x>.
- [45] H. An, Y.G. Choi, Y.R. Jo, H.J. Hong, J.K. Kim, O. Kwon, S. Kim, M. Son, J. Yang, J.C. Park, H. Choi, J. Lee, J. Song, M.H. Ham, S. Ryu, Y. Kim, C.W. Bark, K.T. Ko, B.J. Kim, S. Lee, Experimental realization of strain-induced room-temperature ferroelectricity in SrMnO<sub>3</sub> films via selective oxygen annealing, *NPG Asia Mater.* 13 (1) (2021) 1–10, <http://dx.doi.org/10.1038/s41427-021-00335-7>.
- [46] J. Hirth, Dislocations, steps and disconnections at interfaces, *J. Phys. Chem. Solids* 55 (10) (1994) 985–989, [http://dx.doi.org/10.1016/0022-3697\(94\)90118-X](http://dx.doi.org/10.1016/0022-3697(94)90118-X).
- [47] B.S. Kwak, A. Erbil, J.D. Budai, M.F. Chisholm, L.A. Boatner, B.J. Wilkens, Domain formation and strain relaxation in epitaxial ferroelectric heterostructures, *Phys. Rev. B* 49 (1994) 14865–14879, <http://dx.doi.org/10.1103/PhysRevB.49.14865>.
- [48] J.P. Ruf, H. Paik, N.J. Schreiber, H.P. Nair, L. Miao, J.K. Kawasaki, J.N. Nelson, B.D. Faeth, Y. Lee, B.H. Goodge, B. Pamuk, C.J. Fennie, L.F. Kourkoutsis, D.G. Schlom, K.M. Shen, Strain-stabilized superconductivity, *Nat. Commun.* 12 (1) (2021) 59, <http://dx.doi.org/10.1038/s41467-020-20252-7>.
- [49] S. Gariglio, M. Gabay, J. Mannhart, J.-M. Triscone, Interface superconductivity, *Phys. C: Supercond. Appl.* 514 (2015) 189–198, <http://dx.doi.org/10.1016/j.physc.2015.02.028>.
- [50] O. Diéguez, K.M. Rabe, D. Vanderbilt, First-principles study of epitaxial strain in perovskites, *Phys. Rev. B* 72 (2005) 144101, <http://dx.doi.org/10.1103/PhysRevB.72.144101>.
- [51] H. Ding, S.S. Dwaraknath, L. Garten, P. Ndione, D. Ginley, K.A. Persson, Computational approach for epitaxial polymorph stabilization through substrate selection, *ACS Appl. Mater. & Interfaces* 8 (20) (2016) 13086–13093, <http://dx.doi.org/10.1021/acsami.6b01630>.
- [52] S. Toso, D. Dardzinski, L. Manna, N. Marom, Structure prediction of ionic epitaxial interfaces with Ogré demonstrated for colloidal heterostructures of lead halide perovskites, *ACS Nano* 19 (5) (2025) 5326–5341, <http://dx.doi.org/10.1021/acsnano.4c12713>.
- [53] T. Angsten, L.W. Martin, M. Asta, Orientation-dependent properties of epitaxially strained perovskite oxide thin films: Insights from first-principles calculations, *Phys. Rev. B* 95 (2017) 174110, <http://dx.doi.org/10.1103/PhysRevB.95.174110>.
- [54] Z. Xu, P. Salvador, J.R. Kitchin, First-principles investigation of the epitaxial stabilization of oxide polymorphs: TiO<sub>2</sub> on (Sr,Ba)TiO<sub>3</sub>, *ACS Appl. Mater. & Interfaces* 9 (4) (2017) 4106–4118, <http://dx.doi.org/10.1021/acsami.6b11791>.
- [55] C. Zhou, G.S. Rohrer, P.A. Salvador, Computationally guided epitaxial synthesis of (Sr/Ba)MnO<sub>3</sub> films on (Sr/Ba)TiO<sub>3</sub> substrates, *Comput. Mater. Sci.* 229 (2023) 112415, <http://dx.doi.org/10.1016/j.commatsci.2023.112415>.
- [56] P. Mehta, P.A. Salvador, J.R. Kitchin, Identifying potential BO<sub>2</sub> oxide polymorphs for epitaxial growth candidates, *ACS Appl. Mater. & Interfaces* 6 (5) (2014) 3630–3639, <http://dx.doi.org/10.1021/am4059149>.
- [57] G.S. Rohrer, Grain boundary energy anisotropy: A review, *J. Mater. Sci.* 46 (18) (2011) 5881–5895, <http://dx.doi.org/10.1007/S10853-011-5677-3>.
- [58] A. Tsoga, P. Nikolopoulos, Surface and grain-boundary energies in yttria-stabilized zirconia (YSZ-8 mol%), *J. Mater. Sci.* 31 (20) (1996) 5409–5413, <http://dx.doi.org/10.1007/BF01159310>.
- [59] K. Syed, N.B. Motley, W.J. Bowman, Heterointerface and grain boundary energies, and their influence on microstructure in multiphase ceramics, *Acta Mater.* 227 (2022) 117685, <http://dx.doi.org/10.1016/j.actamat.2022.117685>.
- [60] P. Shewmon, *Energy and structure of grain boundaries*, ASM, 1966.
- [61] G. Herrmann, H. Gleiter, G. Bärö, Investigation of low energy grain boundaries in metals by a sintering technique, *Acta Metall.* 24 (4) (1976) 353–359, [http://dx.doi.org/10.1016/0001-6160\(76\)90100-9](http://dx.doi.org/10.1016/0001-6160(76)90100-9).
- [62] H. Sautter, H. Gleiter, G. Bärö, The effect of solute atoms on the energy and structure of grain boundaries, *Acta Metall.* 25 (4) (1977) 467–473, [http://dx.doi.org/10.1016/0001-6160\(77\)90237-1](http://dx.doi.org/10.1016/0001-6160(77)90237-1).
- [63] U. Erb, H. Gleiter, The effect of temperature on the energy and structure of grain boundaries, *Scr. Metall.* 13 (1) (1979) 61–64, [http://dx.doi.org/10.1016/0036-9748\(79\)90390-9](http://dx.doi.org/10.1016/0036-9748(79)90390-9).
- [64] R. Maurer, Improved technique for the determination of low energy boundaries by the rotating-sphere-on-a-plate method: Results for grain boundaries in the Cu/Ni system, *Acta Metall.* 35 (10) (1987) 2557–2565, [http://dx.doi.org/10.1016/0001-6160\(87\)90153-2](http://dx.doi.org/10.1016/0001-6160(87)90153-2).
- [65] R. Balluffi, R. Maurer, On rotating sphere-on-a-plate experiments and the question of whether high angle grain boundaries melt below bulk melting temperatures, *Scr. Metall.* 22 (5) (1988) 709–713, [http://dx.doi.org/10.1016/S0036-9748\(88\)80187-X](http://dx.doi.org/10.1016/S0036-9748(88)80187-X).
- [66] G. Günther, P. Wilbrandt, P. Haasen, On the formation of low energy grain boundaries in a spheres-on-plate experiment, *Materials Science Forum* 113–115 (1993) 661–666, <http://dx.doi.org/10.4028/www.scientific.net/msf.113-115.661>.
- [67] G. Günther, P.-J. Wilbrandt, The determination of low-energy grain boundaries by the spheres-on-plate experiment in Cu and Cu–0.1 at% Mn, *Phys. Status Solidi (A)* 150 (2) (1995) 635–651, <http://dx.doi.org/10.1002/pssa.2211500207>.
- [68] M. Zieher, A. Tschöpe, R. Birringer, J. Markmann, Examination of the energy phase space of mixed copper grain boundaries by EBSD and the sphere-on-a-plate method, *Acta Mater.* 61 (15) (2013) 5586–5594, <http://dx.doi.org/10.1016/j.actamat.2013.05.042>.
- [69] H. Fecht, H. Gleiter, A lock-in model for the atomic structure of interphase boundaries between metals and ionic crystals, *Acta Metall.* 33 (4) (1985) 557–562, [http://dx.doi.org/10.1016/0001-6160\(85\)90019-7](http://dx.doi.org/10.1016/0001-6160(85)90019-7).
- [70] J. Shirokoff, U. Erb, Detection of the complete set of preferred orientations of silver on sodium chloride, *Scr. Metall.* 20 (11) (1986) 1607–1611, [http://dx.doi.org/10.1016/0036-9748\(86\)90404-7](http://dx.doi.org/10.1016/0036-9748(86)90404-7).
- [71] R. Maurer, H. Fischmeister, Low energy heterophase boundaries in the system silver/nickel and in other weakly bonded systems, *Acta Metall.* 37 (4) (1989) 1177–1189, [http://dx.doi.org/10.1016/0001-6160\(89\)90113-2](http://dx.doi.org/10.1016/0001-6160(89)90113-2).

# Supplementary Information: On the generality of a preferred orientation at interfaces of crystals.

Catherine Zhou<sup>a</sup>, Gregory S. Rohrer<sup>a</sup>, Paul A. Salvador<sup>a,\*</sup>

<sup>a</sup>*Department of Materials Science and Engineering, Carnegie Mellon University, 5000 Forbes Ave., Pittsburgh, 15213, PA, USA*

---

## Abstract

This document primarily provides supplemental figures to the main text (§ S1). The grain boundary energies are for *fcc* Ni are plotted versus  $\Sigma$  values in Figure S1, as reproduced with permission from [1]. A similar plot for *bcc* Fe is given in the main text as Figure 8, as reproduced with permission from [2]. The grain boundary energies are plotted as a function of the angle between the substrate surface plane normal and the normal to the (100) in Figure S2 and S3, for *fcc* Al and *bcc* Mo, respectively. These are respectively similar to Figures 9 and 10 in the main text, which are for *fcc* Ni and *bcc* Fe. The minimum grain boundary energies for a given orientation are plotted as a function of the angle between the substrate surface plane normal and the normal to the (100) in Figures S4 and S5, respectively for *fcc* Al and *bcc* Mo. These are respectively similar to Figures 11a and 11b in the main text, which are for *fcc* Ni and *bcc* Fe. Details of all figures in the supplemental file are explained in the main text, relative to the figures mentioned in this abstract. In addition, examples of planar matches for the  $\Sigma 3$  misorientation are given in § S2, and references cited are given in the Bibliography.

*Keywords:* solid interfaces, epitaxy of thin films, grain boundaries

*PACS:* 68.35.Dv, 68.55.-a, 61.72.Mm

---

---

\*Corresponding Author: paul.salvador@cmu.edu

## S1. Supplemental Figures

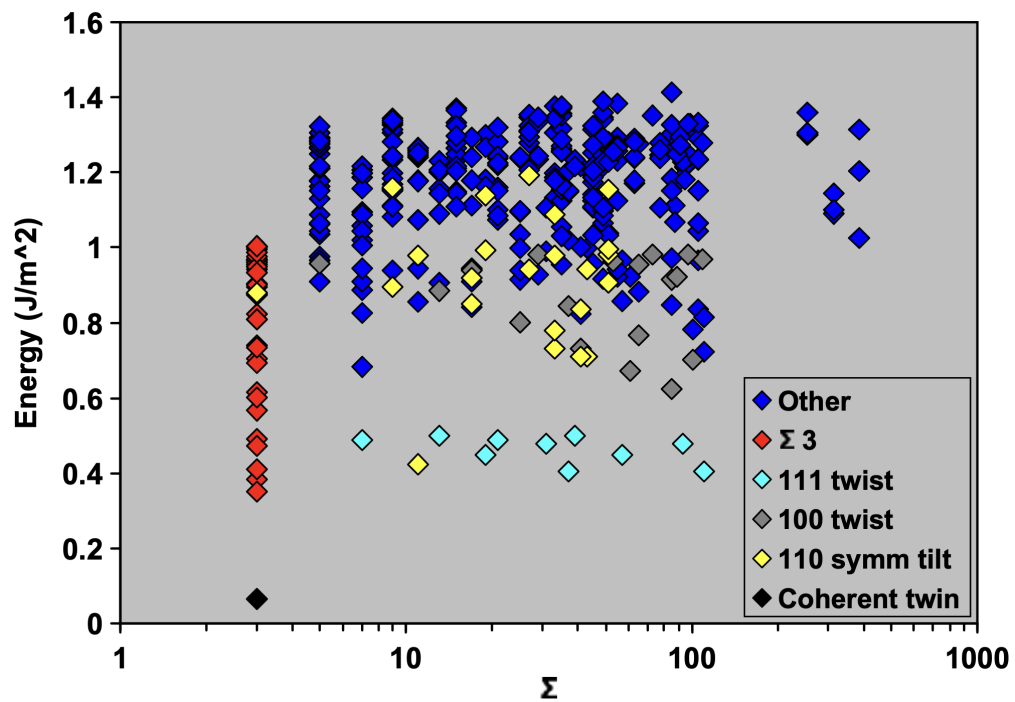


Figure S1: Grain boundary energy plotted as a function of  $\Sigma$  values ( $N$ ) for *fcc* Ni. The legend indicates the planes of select boundaries. Reproduced with permission from [1].

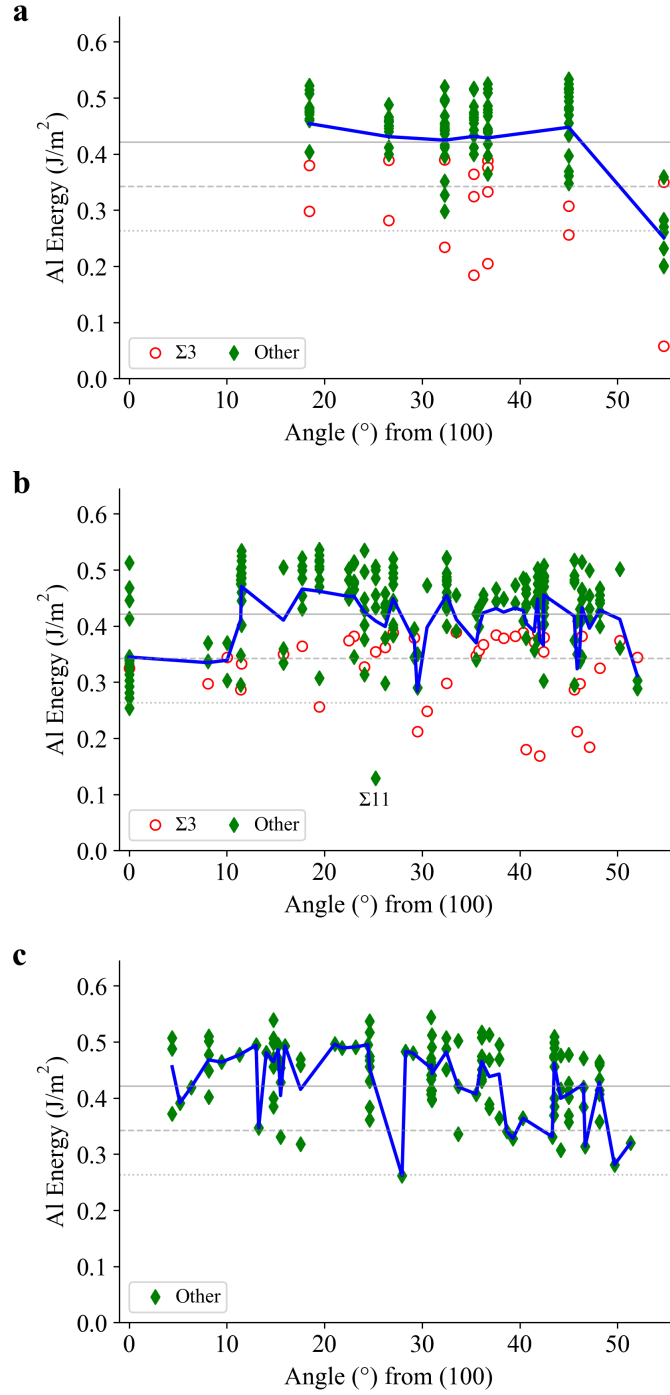


Figure S2: Substrate (left grain boundary orientations) relative to the angle from (100) vs. grain boundary energy (J/m<sup>2</sup>) for *fcc* Al. a), b), and c), are respectively for orientations with two or more, one, and no  $\Sigma 3$  boundaries calculated. Red circles (green diamonds) indicate  $\Sigma 3$  boundaries (all other boundaries). The blue line follows the average energy for each orientation. The gray solid, dashed, and dotted lines are positioned at the global average, one standard deviation less than the global average, and two standard deviations less than the global average, respectively. Figures are explained in the main text.

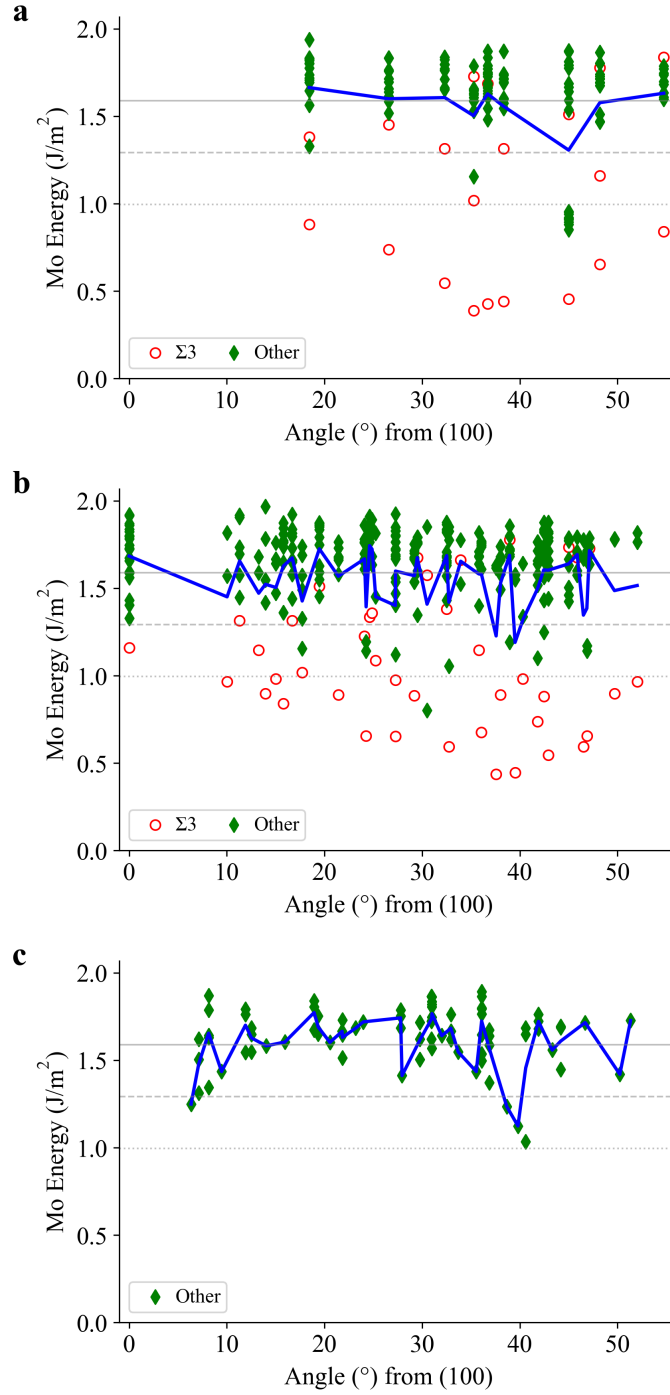


Figure S3: Substrate (left grain boundary orientations) relative to the angle from (100) vs. grain boundary energy ( $\text{J}/\text{m}^2$ ) for *bcc* Mo. a), b), and c), are respectively for orientations with two or more, one, and no  $\Sigma 3$  boundaries calculated. Red circles (green diamonds) indicate  $\Sigma 3$  boundaries (all other boundaries). The blue line follows the average energy for each orientation. The gray solid, dashed, and dotted lines are positioned at the global average, one standard deviation less than the global average, and two standard deviations less than the global average, respectively. Figures are explained in the main text.

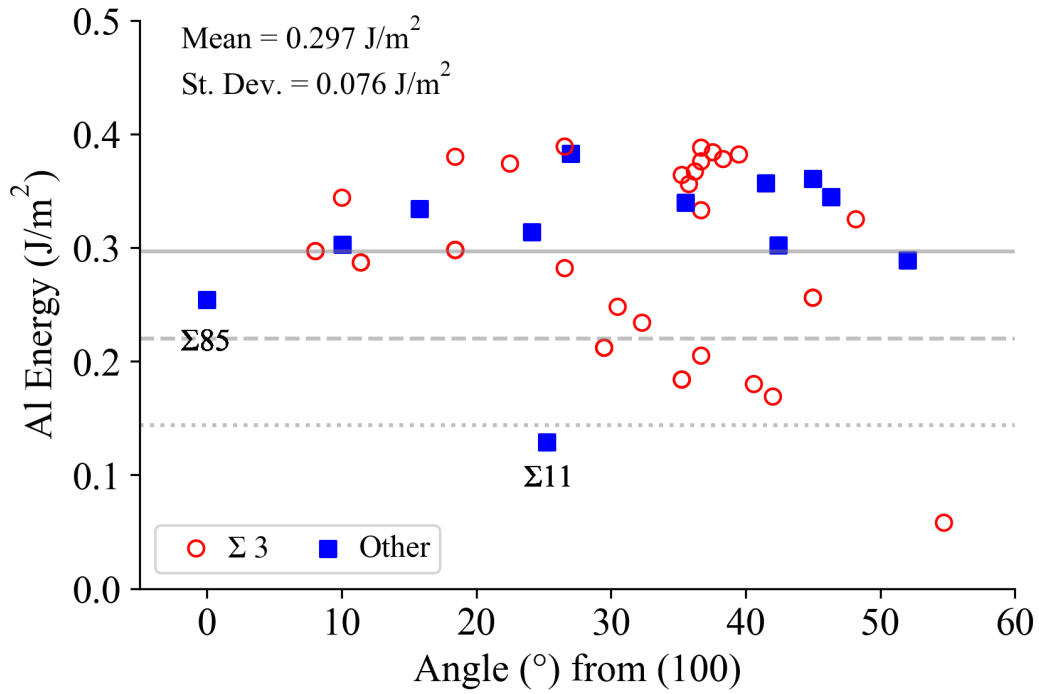


Figure S4: Substrate (left grain boundary orientations) relative to the angle from (100) vs. grain boundary energy (J/m<sup>2</sup>) for the minimum value of a given orientation, for boundaries with 1 or more  $\Sigma 3$  boundaries calculated, for *fcc* Al. Red circles (blue squares) indicate orientations that are  $\Sigma 3$  (other  $\Sigma N$ ) boundaries. The gray solid, dashed, and dotted lines are positioned at the average of minimum energies, one standard deviation less than the average, and two standard deviations less than the average, respectively. Figures are explained in the main text.